Vehicle System Dynamics: International Journal of Vehicle Mechanics and Mobility

Development of a wear model for the wheel profile optimisation on railway vehicles

M. Ignesti [a] , A. Innocenti [a] , L. Marini [a] , E. Meli [a] & A. Rindi [a]

[a] Department of Energy Engineering , University of Florence , via
S. Marta n. 3, 50139 , Firenze , Italy
Published online: 07 Jun 2013.

PLEASE SCROLL DOWN FOR ARTICLE

Taylor & Francis
Taylor & Francis Group

Development of a wear model for the wheel profile optimisation on railway vehicles

M. Ignesti, A. Innocenti, L. Marini, E. Meli* and A. Rindi

Department of Energy Engineering, University of Florence, via S. Marta n. 3, 50139 Firenze, Italy

The modelling and the reduction of wear due to wheel–rail interaction is a fundamental aspect in the railway field, mainly correlated to safety, maintenance interventions and costs. In this work, the authors present two innovative wheel profiles, specifically designed with the aim of improving the wear and stability behaviour of the standard ORE S1002 wheel profile matched with the UIC60 rail profile canted at 1/20 rad, which represents the wheel–rail combination adopted in the Italian railway line. The two wheel profiles, conventionally named CD1 and DR2, have been developed by the authors in collaboration with Trenitalia S.p.A. The CD1 profile has been designed with the purpose of spreading the contact points in the flange zone on a larger area in order to reduce wear phenomena and having a constant equivalent conicity for small lateral displacements of the wheelset with respect to the centred position in the track. The DR2 wheel profile is instead designed to guarantee the same kinematic characteristics of the matching formed by ORE S1002 wheel profile and UIC60 rail profile with laying angle α_p equal to 1/40 rad, widely common in European railways and characterised by good performances in both wear and kinematic behaviour. The evolution of wheel profiles due to wear has been evaluated through a wear model developed and validated by the authors in previous works. The wear model comprises two mutually interactive units: a vehicle model for the dynamic simulations and a model for the wear assessment. The whole model is based on a discrete process: each discrete step consists in one dynamic simulation and one profile update by means of the wear model; within the discrete step, the profiles are supposed to be constant. The choice of an appropriate step is crucial in terms of precision and computational effort: the particular strategy adopted in the current work has been chosen for its capacity in representing the nonlinear wear evolution and for the low computational time required. In the present research, the investigated trainset is the passenger vehicle ALSTOM ALn 501 'Minuetto', which is usually equipped with the standard ORE S1002 wheel profile in Italian railways. The entire model has been simulated on a virtual track specifically developed to represent a statistical description of the whole Italian line. The data necessary to build the virtual track and the vehicle model were provided by Trenitalia S.p.A. and Rete Ferroviaria Italiana. The CD1 and DR2 wheel profiles, matched to the UIC60 rail with cant 1/20 rad, have shown a good behaviour in terms of wear resistance if compared with the old ORE S1002 wheel profile, consequently assuring a more uniform distribution of the removed material and a prolongation of the mean time between two subsequent re-profiling interventions.

Keywords: wear; wheel rail profile; railway systems

1. Introduction

Wear phenomena due to wheel–rail interaction represent a critical aspect in railway applications; in fact, the consequent evolution of rail and wheel profiles involves serious effects on both dynamical and stability characteristics of vehicles. From a safety standpoint, modifications in

---

*Corresponding author. Emails: meli@mapp1.de.unifi.it; enrico.meli@unifi.it

wheel and rail profiles may compromise the vehicle stability and also increase the derailment risk due to wheels climbing over the rail. Profile changes lead also to higher maintenance cost, mainly concerned with the periodically re-profiling operations of wheels and the undesirable replacements of rails, necessary to re-establish the original profiles. A reliable wear model can be used to optimise the original profiles of wheel and rail and to obtain a more uniform wear on rolling surfaces. In such a way the overall amount of worn material can be reduced, the mean time between two maintenance interventions can be increased and, at the same time, the dynamical performance of the wheel–rail pair can be kept approximately constant between two succeeding repair interventions.

The shape optimisation of profiles for the reduction of wear at the wheel–rail interface represents an important aspect in railway field and various approaches were developed to obtain a satisfactory combination of wheel and rail profiles; several works, based on the rolling radii difference, contact angle, equivalent conicity or wheel/rail gap minimisation can be found in the literature.[1–4] The optimum matching is usually pursued through the design of a new wheel profile which matches an existing rail profile, because the cost of rail interventions is notably higher compared with the cost of turning or replacement of the wheels. The optimisation procedure developed by the authors, with respect to the state-of-the-art, introduces innovative features due to the fact that it permits to work directly on the contact points and on their distribution, with a consequent improvement in terms of wear control, stability and guidance.

This paper describes the design procedure and the behaviour in wear reduction of two innovative wheel profiles, developed by the authors in collaboration with Trenitalia and Rete Ferroviaria Italiana (RFI), with the aim of reducing wheel–rail wear that occurs when coupling ORE S 1002 wheel profile and UIC60 rail profile with laying angle α_p equal to 1/20 rad, as it occurs in the Italian line. The two wheel profiles proposed in this paper, conventionally named CD1 wheel profile and DR2 wheel profile,[5] have been designed by means of new wheel shape optimisation procedures, representing one of the main innovative aspects of the present research activity.

CD1 wheel profile has been designed starting from two different purposes. The first consists in spreading the contact points in the flange zone on a larger area to decrease wear phenomena entity. The second purpose is based on obtaining a constant equivalent conicity value in a band around the initial contact point (when the generic wheelset is not shifted from the central position).

The design procedure of DR2 wheel profile aims to keep with the new profile the kinematic characteristics of the matching formed by ORE S1002 wheel profile and UIC60 rail profile with laying angle α_p equal to 1/40 rad, which is commonly adopted in European railways and characterised by good wear and kinematic performances.

The trainset to be investigated in order to evaluate the capability in wear reduction of the two innovative profiles is the passenger vehicle ALSTOM ALn 501 'Minuetto', which is equipped with the standard ORE S1002 wheel profile and UIC60 rail profile canted at 1/20 rad in the Italian railway. This particular vehicle exhibited a poor wear performance, as verified by experimental measurements when operated in the Aosta Pre-Saint Didier track.

The evolution of wheel profiles has been evaluated by means of a model specifically developed for the wear assessment, which has been validated by the authors in previous works [6,7] in collaboration with Trenitalia S.p.A. and RFI, which provided the experimental data relating to some tests performed with the vehicle to be investigated on the Aosta-Pre Saint Didier line.[5] This rail road turned out to be quite critical for its sharpness and for the characteristics of the 'Minuetto', when operated on that railway track. The model validation has been performed evaluating and comparing the reference quotas of the wheel profile [8] with respect to the experimental values.

The general architecture of the developed wear model comprises two mutually interactive parts: the *vehicle model* (multibody model and three-dimensional (3D) global contact model) and the *wear model* (local contact model, wear estimation and profiles updating).

The multibody model of the vehicle is implemented in the Simpack Rail environment and it takes into account all the significant degrees of freedom of the vehicle. The 3D global contact model, developed by the authors in previous works,[9,10] detects the wheel–rail contact points by means of an innovative algorithm based on suitable semi-analytical procedures and then, for each contact point, calculates the contact forces by means of Hertz's and Kalker's theory.[11–13] Thanks to the numerical efficiency of the new contact model, it can interact directly online with the multibody model during the dynamic simulation of the vehicle, without look-up table with saved pre-calculated values of contact parameters.

Wear evolution is performed by means of a model based on a local contact model (in this case, the Kalker's FASTSIM algorithm) and on an experimental relationship for the calculation of the worn material available in the literature [14–16] (based on the work of the frictional forces). The wear model, starting from the outputs of the vehicle model (contact points, contact forces and global creepages), is able to calculate the total amount of removed material due to wear in dry conditions and its corresponding distribution along the wheel profile. Since the aim of the present research activity consists in the optimisation of wheel profile, only wheel wear is considered and the evolution of a single-mean wheel profile for the whole vehicle is studied. The removal process of the material takes into account the 3D structure of the contact bodies.

The evolution of wheel profiles due to wear is a key aspect in railway research field as proven by the raising number of research groups dealing with this issue. In the literature, many important research works regarding wear models based on global and local approaches for the wear evaluation can be found. The global approach,[17,18] commonly adopted by commercial multibody software (e.g. Simpack), evaluates wear progress without taking into account the contact patch, but hypothesising a single-point contact. This approach leads to lower computational times, disregarding the model accuracy with consequent possible overestimation or underestimation of worn material. Local wear computation approaches [6,14–16] use instead local wheel–rail contact models, wherein a transverse wheel wear distribution is allowed; the model accuracy is improved with a consequent disadvantageous increase in computation time. Local and global approaches have also been compared in interesting works.[19] According to the state-of-the-art, a substantial lack is present in the literature concerning wear models (both global and local) specifically developed for complex railway net applications. In such a case, the computational effort required to run the exhaustive simulation of vehicle dynamics and wear evaluation turns out to be absolutely too high for each practical purpose.

It is worth noting that the innovative wear model is not used during the wheel profiles design and optimisation phase (which is based on kinematic considerations); the wear model is employed at a later stage to assess the performance in terms of wear of the new wheel profiles.

In the present work, the authors present an innovative statistical approach to perform wear analysis on complex railway track in reasonable computational time for practical purpose, representing an innovative aspect in wheel wear research field.

Therefore, all the simulations are performed on a virtual track, specifically designed to represent a statistical description of the whole Italian railway line.[5] This statistical railway line is a set of N_c curvilinear track characterised, as it will be explained in the following sections, by a specific radius R, superelevation h, velocity V and statistical weights p_k, representing the occurrence frequency of each curvilinear track with respect to the entire investigated line (with $1 \leq k \leq N_c$).

The rail profiles have been considered constant; in particular, a set of mean constant worn rail profiles (in statistical sense) has been adopted to be associated with the curvilinear tracks

of the statistical railway line. This set has been obtained through a statistical analysis of the entire Italian railway network.

2.   General architecture of the model

The general architecture of the model consists in a discrete procedure articulated in two separate parts that work alternatively at each procedure step: the *vehicle model* and the *wear model*. The general layout of the entire model is illustrated in the diagram in Figure 1. The *vehicle model* is the part responsible for the dynamical simulations and it is based on the online mutual interaction of the multibody model of the vehicle to be investigated (in this work the ALSTOM ALn 501 'Minuetto'), the characteristics of the investigated track, the relative operating conditions and the 3D global contact model. More specifically, at each integration step during time-domain dynamic simulation, the multibody model evaluates the kinematic variables (position, orientation and their derivatives) of the considered vehicle at each wheelset. These variables are then passed to the 3D global contact model, whose task consists in the calculation of the global contact parameters: contact points, contact areas, global creepages and contact forces. In particular, the contact points detection is based on an innovative algorithm developed by the authors in previous works,[6,9,10] while the contact forces (normal and tangential forces) calculation is performed according to Hertz's and Kalker's global theories.[11–13] Once the tangential contact problem has been solved, the values of the global forces are sent back to the multibody model and the dynamical simulation proceeds with the next time integration step.
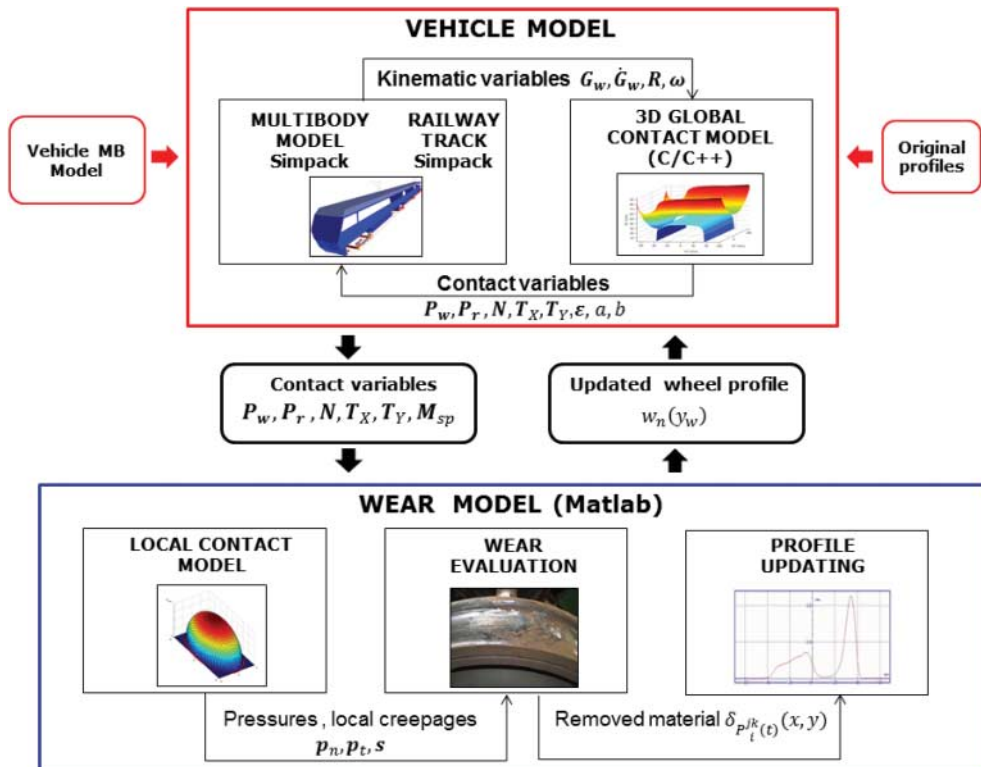

Figure 1.   General architecture of the model.

The inputs of the multibody model are the geometrical and inertial properties of the considered railway vehicle. The geometrical inputs of the 3D global contact model are wheel and rail original profiles described by means of discrete sets of points. During this research project, according to the specifications required by Trenitalia, the capability on wear reduction of two innovative wheel profiles has been evaluated. Each of these profiles (CD1 and DR2 wheel profiles designed by the authors in collaboration with Trenitalia and RFI [5]) fits the considered vehicle in a specific simulation set.

The *vehicle model* for the simulations has been modelled in the commercial Multibody Software Simpack. In particular, the multibody model has been defined in the Simpack Rail environment, while the wheel–rail 3D global contact model has been implemented in a subroutine written in C language. This subroutine is called by a specifically developed FORTRAN routine defined within the Simpack *User routines* module, which allows the customisation of the contact model employed in the dynamical simulations.

The *wear model* is the part of the procedure concerning the computation of wheel profile evolution and it predicts the amount of worn material to be removed from the wheel surfaces. The wear model can be sub-divided into three parts: the local contact model, the evaluation of worn material and the profile updating. First, the local contact model (whose approach is based on Hertz's local theory and Kalker's simplified theory implemented in FASTSIM algorithm) estimates the local contact pressures and creepages and detects the creep zone of the contact area. Then, according to an experimental relationship between the worn material and the energy dissipated by friction forces at the contact interface,[14–16] the quantity of removed material on wheel surface is computed on the creep area. This estimation is performed hypothesising dry contact friction at the wheel–rail interface as Trenitalia and RFI requirements establish. The last step of the wear prediction procedure consists in updating the profiles: the worn profiles are derived from the original ones using an appropriate update strategy. The single-mean profile $w_n(s)$ (the same one for all the vehicle) is then fed back as input to the entire *vehicle model* and the whole model procedure proceeds with the next discrete step.

In the present work, the total mileage to be simulated km_{tot} is subdivided into several steps characterised by a value km_{step} of the travelled distance and the wheel profiles are supposed to be constant within each discrete step. It is worth noticing that a decrease of the km_{step} value increases the model precision and, at the same time, the computational effort.

The adopted updating strategy for the km_{step} choice is a key point since it may appreciably affect the results and its main task consists in evaluating the mileage after which wheel profiles should be updated, that is the distance km_{step} simulated during each discrete step. Different updating strategies are available in the literature and the most significant are

- the constant step update strategy,[20,21] which is characterised by a constant value km_{step} of the discrete step;
- the adaptive step update strategy,[6,14,16] wherein the wheel profile is updated when a given threshold of the maximum value of cumulative wear depth is reached and the value km_{step} is consequently variable.

During this research activity, the adaptive step has been adopted for its capacity in representing the nonlinear behaviour of the wear evolution. In the first phase of the simulations, when the interaction between wheel and rail unworn profiles is represented by non-conformal contact, the wear evolution is characterised by a higher rate. In the second phase, a slower rate due to the more conformal contact is present. Furthermore, this strategy presents computational times comparable with those relative to the constant step update strategy.

The entire *wear model* has been implemented in the Matlab environment.

Table 1. Main characteristics of the Aln 501 Minuetto DMU.

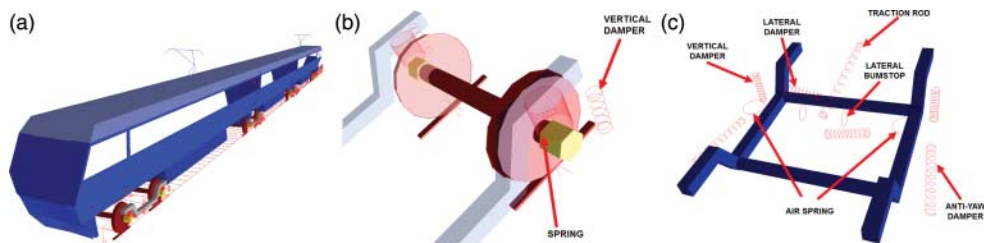|	
Length	51.9 m
Width	2.95 m
Height	3.82 m
Bogie pivot distances	14.8–13.8–14.8 m
Bogie wheelbase	2.80 m
Unladen weight	100 t
Wheel arrangement	Bo-2-2-Bo
Wheel diameter	850 mm
Max speed	130 km/h

Figure 2. Multibody model of the vehicle. (a) Global view, (b) primary suspensions, (c) secondary suspensions.

2.1. *The vehicle model*

The present section deals with the description of the *vehicle model*. First of all, the multibody representation for the dynamical simulations of the studied vehicle is introduced. Then, the algorithm that models the 3D global contact is briefly explained.

2.1.1. *The multibody model*

The trainset investigated during this research is ALSTOM ALn 501 'Minuetto', a passenger transport unit widespread in Italian Railways, equipped with the standard ORE S1002 wheel profile and UIC60 rail profile canted at $1/20$ rad. This particular vehicle exhibits in fact severe wear and stability problems mainly caused by the adopted matching. Its mechanical structure and inertial, elastic and damping properties can be found in the literature.[5] Table 1 shows the main characteristics of the considered vehicle.

The multibody model of the vehicle has been implemented in the Simpack environment (Figure 2(a)) and it mainly consists of car bodies connected by means of the secondary suspensions to the vehicle bogies, which in turn are linked to wheelsets through the primary suspensions. Totally, the multibody model is made up of 31 rigid bodies:

- 3 coaches;
- 4 bogies: 2 external motor bogies and 2 intermediate trailer bogies interposed between 2 successive coaches;
- 8 wheelsets: 2 for each bogie;
- 16 axle boxes: 2 for each wheelset.

The inertial characteristics of the vehicle are listed in Table 2: it should be noticed that motors and gear boxes are not represented by an opposite body in the multibody model and their inertial properties have been included in the motor bogie frame and in the wheelset bodies.

Table 2. The Aln 501 Minuetto main inertial properties.

	Mass kg	I_{xx} kg m^2	I_{yy} kg m^2	I_{zz} kg m^2	z_{CoG} m
External coach	31,568	66,700	764,000	743,000	−1.91
Internal coach	14,496	30,600	245,000	236,000	−1.98
Motor bogie frame	3306	1578	2772	4200	−0.5
Trailer bogie frame	3122	1647	3453	5011	−0.5
Wheelset	2091	1073	120	1073	−0.425

Table 3. Main linear stiffness properties of the ALn 501 'Minuetto'.

Primary suspension	Flexicoil k_z	9.01×10^5 N/m
	Flexicoil k_x, k_y	1.26×10^6 N/m
	Sutuco bushing k_x	2.0×10^7 N/m
	Sutuco bushing k_y	1.5×10^7 N/m
Secondary suspension	Airspring k_z	3.98×10^5 N/m
	Airspring k_x, k_y	1.2×10^5 N/m
	Anti-roll bar k_α	2.6×10^6 Nm/rad
Coach connection	Bushing k_x, k_z	7.24×10^7 N/m
	Bushing k_y	5.2×10^6 N/m

The dual-stage suspensions have been modelled by means of 3D linear and nonlinear visco-elastic force elements. In the primary suspension stage, the elastic elements are Flexicoil springs (constituted by two coaxial helical compression springs), while damping of the vertical relative displacement is provided by means of two nonlinear dampers (Figure 2(b)).

The secondary stage (Figure 2(c)) is formed by pneumatic suspensions and it comprises the following elements:

- two air springs;
- six nonlinear dampers (lateral, vertical and anti-yaw dampers);
- one nonlinear traction rod;
- the roll bar (not visible in the figure);
- two nonlinear lateral bumpstops.

The main linear properties of the suspensions are given in Table 3.

2.1.2. *3D global contact model*

The aim of any formulation describing the wheel–rail contact mechanism consists in an accurate prediction of the contact points location, whose determination is fundamental to correctly evaluate the contact forces and the consequent dynamical behaviour of the vehicle. In this research activity, a specifically developed 3D global contact model has been employed in order to improve the reliability and accuracy of the contact points detection, compared to those given by the Simpack Rail contact model. As shown in Figure 1, the global contact model inputs are the kinematic variables evaluated by the multibody model, i.e. the position, the orientation matrix R_w^r, the absolute velocity $\dot{\mathbf{O}}_w^r$ and the absolute angular velocity $\boldsymbol{\omega}_w^r$ of the wheelset. Starting from these inputs, the global contact model developed by the authors evaluates the following outputs: positions $\mathbf{P}_w^r$ and $\mathbf{P}_r^r$ of the contact points, the normal $\mathbf{N^r}$ and tangential $\mathbf{T_x^r}$ and $\mathbf{T_y^r}$ contact forces (Figure 3), the global creepages $\boldsymbol{\varepsilon}$ and the contact patch's dimensions a, b. The subscripts w and r refer, respectively, to appropriate reference
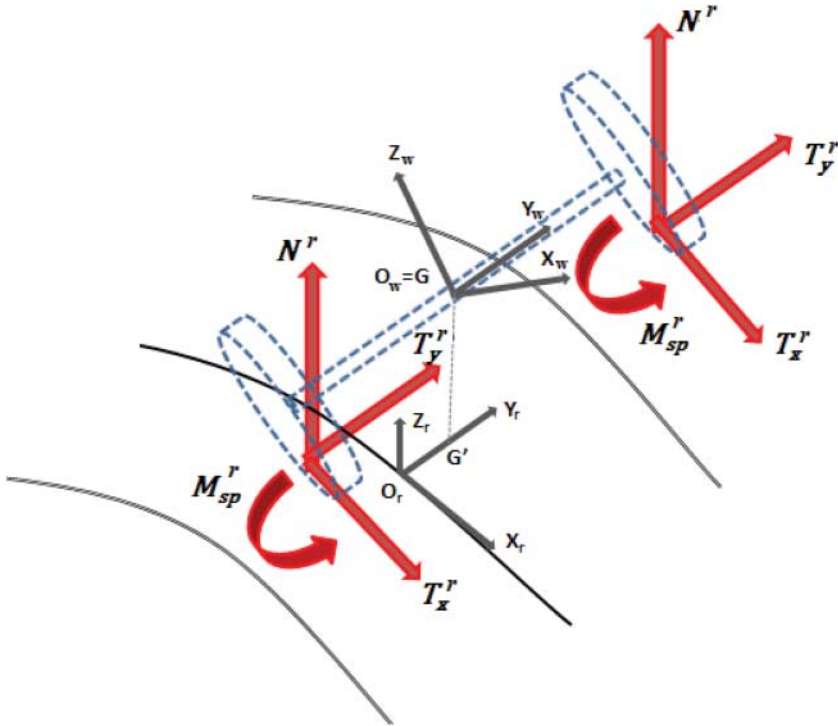
Figure 3. Global forces acting at wheel and rail interface.

systems that will be introduced in Section 4.2.1. According to these reference systems, wheel and rail profiles can be, respectively, defined as $w(y_w)$ and $r(y_r)$. In particular, the adopted contact model is based on a two-step procedure; at the first step the contact points number and positions are determined through an innovative algorithm designed and validated by the authors.[6,9,10] During the second step, for each detected contact point, the global contact forces (Figure 3) are evaluated using Hertz's and Kalker's global theories.[11–13]

The 3D global contact model developed by the authors is based on the analytical reduction of the algebraic contact problem dimension by means of exact analytical procedures, that leads to an increase in accuracy and numerical efficiency of the contact model. Therefore, it is possible to get much closer to the limit condition of conformal contact, when Hertz's and Kalker's theories are not valid without any particular numerical instability. Moreover, when the conformal contact condition is reached, the global contact models may be also replaced by finite element (FE) contact models, able to guarantee the required accuracy.[22,23] These FE contact models, specifically developed for railway research field, ensure high numerical efficiency.

2.2. *The wear model*

The current section deals with the description of the three phases constituting the wear model: the local contact model, the computation of the amount of worn material in dry contact conditions and the wheel profile update. The wear model takes into account normal friction wear, in agreement with Trenitalia. At this phase of the research activity, other wear mechanisms, such as the fatigue pitting wear and the plastic wear, are not considered.

2.2.1. *The local contact model*

The inputs of the wear model are the global contact parameters estimated by the vehicle model. Since a local wear computation is required, the global contact parameters need to be post-processed and this can be achieved with the simplified Kalker's theory implemented in the FASTSIM algorithm. This theory starts from the global creepages (ε), the normal and tangential global forces ($\mathbf{N^r}$, $\mathbf{T_x^r}$, $\mathbf{T_y^r}$), the contact patch dimensions (a, b) and the material properties to compute the local distribution of normal p_n and tangential $\mathbf{p}_t$ stresses and local creepages $\mathbf{s}$ across the wheel–rail contact area. For a more detailed description of the FASTSIM algorithm, one can refer to the literature.[24]

2.2.2. *The wear computation*

The distribution of worn material on wheel profile due to wear (assuming dry contact conditions) is evaluated by means of a wear experimental function, based on a law that relates the energy dissipated in the wheel–rail contact patch with the amount of worn material.[14,15]

The adopted wear function uses local contact normal p_n and tangential $\mathbf{p}_t$ stresses, creepages $\mathbf{s}$ and the vehicle velocity V as the input to compute directly the specific volume of worn material $\delta_{P_{wi}^{jk}(t)}(x, y)$ (mm^3/mm mm^2) related to the ith contact point $P_{wi}^{jk}(t)$ on the jth wheel relative to the kth dynamical simulation for unit of distance travelled by the vehicle (expressed in m) and for unit of surface (expressed in mm). More specifically, local contact stresses and creepages are used to evaluate the *wear index I_W* (expressed in N/mm^2), which represents the frictional power developed by the tangential contact pressures:

$$I_W = \frac{\mathbf{p}_t \bullet \mathbf{s}}{V}. \tag{1}$$

This index can be correlated with the *wear rate K_W* which represents the mass of removed material (expressed in μg/m m^2) for unit of distance travelled by the vehicle and for unit of surface. The correlation chosen for the development of the present wear model is based on real data available in the literature,[14] which have been acquired from experimental wear tests carried out in the case of metal-to-metal contact with dry surfaces using a twin-disc test arrangement. The experimental relationship between K_W and I_W is able to represent three wear regimes: mild, intermediate and severe wear according to the following equation:

$$K_W(I_W) = \begin{cases} 5.3 * I_W & I_W < 10.4 \\ 55.12 & 10.4 \leq I_W \leq 77.2 \\ 61.9 * I_W - 4778.68 & I_W > 77.2. \end{cases} \tag{2}$$

Once the wear rate $K_W(I_W)$ has been computed, the corresponding specific volume of worn material (for unit of distance travelled by the vehicle and for unit of surface) can be calculated as follows (expressed in mm^3/m mm^2):

$$\delta_{P_{wi}^{jk}(t)}(x, y) = K_W(I_W) \frac{1}{\rho}, \tag{3}$$

where ρ represents the material density (expressed in kg/m^3).

2.2.3. *Profile update and smoothing*

After obtaining the amount of worn material, wheel profile need to be updated and then it can be used as the input of the next dynamic simulation. The new profile, denoted by $w_n(y_w)$, is
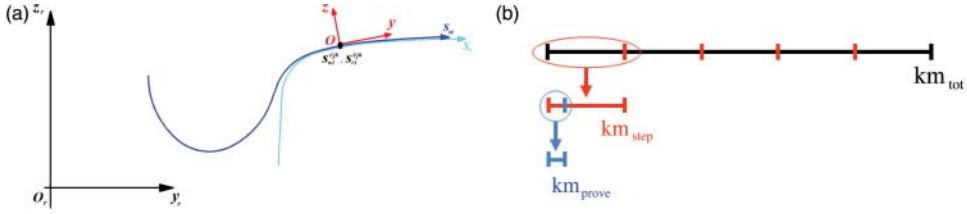
Figure 4. Wear model. (a) Normal abscissa for the wheel and rail profile, (b) discretisation of the total mileage.

computed from the old one $w_o(y_w)$ and from all the calculated distributions $\delta_{P_{wi}^{jk}(t)}(x, y)$ of worn material through an appropriate set of numerical procedure that defines the update strategy. The update strategy is also applied with the aim of reducing the numerical noise characterising the distribution $\delta_{P_{wi}^{jk}(t)}(x, y)$ that can generate problems to the global contact model because of the presence of non-physical alterations in new profiles.

Another issue to be provided from the update procedure is the average of the worn material distributions. In fact, according to Trenitalia and RFI requirements, the output of the wear model must be a single profile; hence, the evaluated distribution $\delta_{P_{wi}^{jk}(t)}(x, y)$ needs to be mediate.

The whole numerical procedures which compute the new profiles can be summed up in the following steps:

(1) *Longitudinal integration*:

$$\frac{1}{2\pi w(y_{wi}^{jk})} \int_{-a(y)}^{+a(y)} \delta_{P_{wi}^{jk}(t)}(x, y) \, dx = \delta_{P_{wi}^{jk}(t)}^{tot}(y); \tag{4}$$

the previous integration provides the mean value of wheel worn material expressed in $mm^3/m\,mm^2$. More specifically, the operation sums in the longitudinal direction all the wheel wear contributions inside the contact path and distributes the resulting quantity along the wheel circumference of length $2\pi w(y_{wi}^{jk})$.

(2) *Time integration*:

$$\int_{T_i}^{T_e} \delta_{P_{wi}^{jk}}^{tot}(y) V(t) \, dt \approx \int_{T_i}^{T_e} \delta_{P_{wi}^{jk}}^{tot}(s_w - s_{wi}^{cjk}(t)) V(t) \, dt = \Delta_{P_{wi}^{jk}}(s_w), \tag{5}$$

where the natural abscissa s_w relative to the curve $w(y_w)$ has been introduced. The following relations locally hold (Figure 4(a)):

$$y \approx s_w - s_{wi}^{cjk}(t) \qquad w(y_w) = w(y_w(s_w)) = \tilde{w}(s_w). \tag{6}$$

The natural abscissa of the contact point s_{wi}^{cjk} can be evaluated starting from its position P_{wi}^{jk}. The integration (5) sums all the wear contributions relative to the dynamic simulation and gives as output the depth of worn material due to the considered contact point $\Delta_{P_{wi}^{jk}}(s_w)$ in $mm = mm^3/mm^2$.

(3) *Sum on the contact points*:

$$\sum_{i=1}^{N_{PDC}} \Delta_{P_{wi}^{jk}}(s_w) = \Delta_{jk}^w(s_w), \tag{7}$$

where N_{PDC} represents the maximum number of contact points that can be considered for each single wheel. The output $\Delta_{jk}^w(s_w)$ is the removed material of the *j*th wheel during

the kth simulation. The number of active contact points changes during the simulation but it is usually less than N_{PDC}; thus, the amount of worn material due to non-active contact points is automatically set equal to zero.

(4) *Average on the vehicle wheels and on the dynamic simulations*:

$$\sum_{k=1}^{N_c} p_k \frac{1}{N_w} \sum_{j=1}^{N_w} \Delta_{jk}^w(s_w) = \bar{\Delta}^w(s_w), \tag{8}$$

where N_w is the number of vehicle wheels, while the p_k, $1 \leq k \leq N_c$, $\sum_{k=1}^{N_C} p_k = 1$ are the statistical coefficients related to the various dynamic simulations. These coefficients have been established by the statistical analysis as will be better explained in the following sections. The average on the number of wheel–rail interactions has to be performed to obtain as output of the wear model a single-average profile for the wheel (as required by Trenitalia and RFI).

(5) *Scaling*: Since it normally takes travelled distance of thousands kilometres in order to obtain measurable effects of wheel wear, an appropriate scaling procedure is necessary to reduce the simulated track length with a consequent limitation of the computational effort. The total mileage km_{tot} travelled by the vehicle is chosen according to the purpose of the simulations, for example equal to the re-profiling intervals. This mileage is subdivided in discrete steps characterised by a length equal to km_{step} and the wheel profile is supposed to be constant within each discrete step (corresponding to a travelled distance equal to km_{step}). The km_{step} value represents a distance which is still too long to be simulated in reasonable computational times.

Assuming that a linear relationship between the amount of worn material and the travelled distance holds within a single step km_{step} of the discrete procedure, it is possible to amplify the quantity of removed material by a suitable scaling factor. The almost linearity characterising the wear model inside a discrete step (the length of which is defined in this work by means of an adaptive strategy based on a given threshold on maximum value of the cumulated wear depth) represents a working hypothesis coming from the discrete approach of the model. It comes from the idea that the wear rate characterising the distance km_{prove} simulated during the considered discrete step remains the same also inside the entire discrete step km_{step}, due to the fact that the vehicle always covers the same railway tracks of the statistical analysis both during the performed simulations km_{prove} and during the entire discrete step km_{step}. Therefore, a smaller distance km_{prove} can be simulated and the relative amount of wheel worn material can be amplified in order to evaluate the worn material distribution relative to a km_{step} travelled distance. Obviously, this hypothesis is meaningful only if the km_{step} value is low enough to ensure that wheel profile variation (due to wear) inside it can be neglected.

As already stated, the discrete step km_{step} definition can be done according to the following two main update strategies:

- the constant step update strategy,[20,21] which is characterised by a constant value km_{step} of the discrete step;
- the adaptive step update strategy,[6,14,16] wherein the profile is updated when a given threshold Δ_{fix} on the maximum value $\Delta_{max} = \max_{s_w} \bar{\Delta}(s_w)$ of cumulative wear depth is reached; the value km_{step} is consequently variable.

During this research activity, the adaptive step has been adopted for its capacity in representing the nonlinear behaviour of the wear evolution. In the first phase of the simulations, when the interaction between wheel and rail unworn profiles is represented by non-conformal contact, the wear evolution is characterised by a higher rate. In a second phase, a slower rate due to the more conformal contact is presented. Furthermore, this strategy

presents computational times comparable with those relative to the constant step update strategy. The discrete step value km_{step} can be defined through the following equation:

$$km_{step} = km_{prove} \frac{\Delta_{fix}}{\Delta_{max}}, \qquad (9)$$

where $km_{prove} = l_{track}$ is the total travelled distance simulated during the N_c dynamic analysis. The quantity Δ_{max} represents the maximum cumulative wear depth, while Δ_{fix} is the related chosen threshold value and in this work it is equal to 0.1 mm. The scaled amount $\bar{\Delta}^{sc}(s_w)$ of worn material to be removed by the wheel surface is then given by the following expression:

$$\bar{\Delta}^{sc}(s_w) = \bar{\Delta}(s_w) \frac{\Delta_{fix}}{\Delta_{max}}. \qquad (10)$$

(6) *Smoothing of the worn material*:

$$\Im[\bar{\Delta}^{wsc}(s_w)] = \bar{\Delta}^{wsc}_{sm}(s_w) \qquad (11)$$

the numerical noise and short wavelengths without physical meanings that may affect the worn material distribution can be passed to the new wheel profile $\tilde{w}_n(s_w)$ with consequent problems raising in the global contact model. Hence, an appropriate smoothing of the worn material distributions is required and this is achieved by means of a first-order discrete filter [25] (i.e. a moving average filter characterised by a window size equal to 1–5% of the total number of points in which the profiles are discretised). This kind of discrete, characterised by high numerical efficiency and simplicity, permits to conserve the mass of the material removed by wear.

(7) *Profile update:*

$$\begin{pmatrix} y_w(s_w) \\ \tilde{w}_o(s_w) \end{pmatrix} - \bar{\Delta}^{wsc}_{sm}(s_w) \mathbf{n}^r_w \xrightarrow{\text{re-parameterisation}} \begin{pmatrix} y_w(s_w) \\ \tilde{w}_n(s_w) \end{pmatrix} \qquad (12)$$

the last step of the procedure consists in the determination of the new wheel profile $\tilde{w}_n(s) = w_n(y)$ starting from the old one $\tilde{w}_o(s) = w_o(y)$. Due to the fact that the removal of material occurs in the normal direction to the profiles ($\mathbf{n}^r_w$ is the outgoing unit vector for the wheel profile), once the quantity $\bar{\Delta}^{wsc}_{sm}(s_w)$ has been removed, a re-parameterisation of the profile must be performed to get curve parameterised by means of the curvilinear abscissa.

3. Setting-up of the Minuetto virtual track

The present section is a brief overview on the procedure used in deriving a significant statistical description of the Italian railway track, an essential task to make possible and rationalise the approach and the simulation work on a complex railway line. Such an approach is especially useful if on the considered railway net many vehicles operate covering different routes.

3.1. *The statistical approach*

When the wear analyses have to be carried out on a set of tracks of considerable length by using at the same time accurate models for the vehicle and the wheel–rail contact, the utilisation of a 'railway line statistical model' may be a indispensable way to overcome a series of problems

Table 4.   Percentage of analysed data for the Minuetto vehicle.

District area	Analysed distance (km)	Total distance (km)	%
Florence	15,576	37,043	42.0
Turin	52,220	78,358	66.6
Naples	16,740	32,939	50.8
Verona	15,182	22,715	66.8
Total	85,719	171,055	50.1

due to the computational times and the organisation of the simulations themselves. The basic idea is to substitute a complex railway net or the too long tracks to be simulated with a set of simpler tracks which can produce an equivalent amount and distribution of wear on the vehicle wheels. The need of a similar approach is even higher if the wear analyses have to be carried out from a wheel profile optimisation point of view; a complete study, considering in detail the characteristics of the thousands of kilometres covered by the vehicles (curve radius, superelevation, speed) would imply a relevant number of simulations and unacceptable computational times, where besides the contribution of each simulation might be not much significant. In such cases, it is fundamental to sum up in a statistical model of the whole railway net the most relevant information about the real context on which the vehicles operate, in order to get results in terms of average behaviour of the vehicle–wheel profile matching considered. In the following, the resultant statistical arrangement of the real tracks (or of the railway net) will be indicated, for the sake of brevity, with expressions such as 'virtual track' or 'mean line'.

In the present work, the statistical approach has been exploited to draw up the mean line of the Minuetto train. This mean line had to be a significant and equivalent synthesis, in a statistical sense, of the whole set of tracks in Italian railways on which the train composition operates every day. The same strategy has also been used in drawing up a virtual track of the Aosta-Pre Saint Didier line aimed at the model validation via comparison with the available experimental results.[6,7]

The methodology is based on the knowledge and the exhaustive analysis of the tracks on which the vehicles operate as well as the relative number of weekly shifts. The shifts are arranged by the district areas of administrative competence of the overall considered railway net of the Minuetto, which are four: Florence, Turin, Verona and Naples. The whole data were made available by Trenitalia S.p.A. and RFI. as electronic databases, paper plans and paper charts of the single tracks. The extent of the analysed data for each district area is summarised in Table 4, where actually the distances are the sum of the products between the length of the sections and the relative number of weekly shifts, to take into account the service frequency in each track. The percentage value is the analysed distance with respect to the total mileage travelled by the vehicle and it represents the completeness of the performed analysis.

Since the idea is to obtain a set of simple right curved tracks, each of them characterised by curve radius, superelevation height and a travelling speed, as a first step the whole data for each vehicle have been grouped in radius classes, according to the classification given in Table 5. The criterion on which the table have been generated is the rigid angle of attack of wheelsets, that is, the difference in yaw angle between the effective position of the wheelset in the track and the radial position by assuming zero equivalent yaw flexibility in the primary suspensions stage. Consequently, the rigid attack angle is a theoretical borderline case which represents the worst possible condition of guidance because the bogie (or the vehicle, if it is a two-axle vehicle) follows the track maximising the travelling resistance and the wear in negotiating curves. Conversely, the radial position is usually the condition through which the resistance and the consequent wear are minimised, not to mention the significant benefits

Table 5.　Classification intervals.

Max rigid angle (mrad)	Min rigid angle (mrad)	Minradius R_m (m)	Maxradius R_M (m)	Meanradius R_r (m)
6.0	5.5	227	208	217
5.5	5.0	250	227	238
5.0	4.5	250	278	263
4.5	4.0	278	313	294
4.0	3.5	313	357	333
3.5	3.0	357	417	385
3.0	2.5	417	500	455
2.5	2.0	500	625	556
2.0	1.5	625	833	714
1.5	1.0	833	1250	1000
1.0	0.5	1250	2500	1667
0.5	0.0	2500	10,000	5000
0.0	0.0	1000	∞	∞

in safety against derailment, since even the longitudinal position of the contact patch on the flange of the external wheel is strongly reduced to almost zero.

The rigid attack angle depends only on the bogie wheelbase and the radius of the curve and for this reason it is only an index to classify qualitatively the hypothetical wear severity of curved tracks. The rigid angle attack should not be confused with the effective steady angle of attack of wheelsets in curve (real or in simulation), which depends on other several parameters of the bogie (yaw stiffness, geometric quantities, etc.) as well as the wheel–rail contact condition (friction coefficient); moreover, each wheelset has its own steady angle of attack depending on the position in the bogie (trailing or leading wheelset). The rigid angle represents a superior limit of the steady angle of attack when the yaw stiffness provided by the primary suspensions (due to a couple of longitudinal stiffness elements which link each axle box to the bogie frame) tends to infinitive. Bogies designed for high speed trains, having a remarkable stiffness in the primary suspensions tends to generate angle of attacks similar to the correspondent rigid angle in negotiating sharp curves. On the contrary, the opposite situation, that is an angle of attack equal to zero, is rarely verified notably for the leading wheelset of a bogie, because it would require a zero yaw stiffness, and this, for reasons due to requirement of stability of the vehicle at high speed, cannot be accepted. Table 5 has been drawn up considering a bogie wheelbase equal to 2.5 m and a step of 0.5 mrad between each class. The reference radius of each class (R_r) has been simply calculated as the weighted average between the radii included in the class interval $[R_m, R_M]$, using as weights the products between the lengths of the track sections and the number of weekly shifts.

In the statistical approach, it is assumed that the wear evolution can be reproduced with a series of simulations on steady curves and straight tracks, neglecting the contribution of the transition lengths (parabolic curves and clothoids [26]) used to connect sections having different superelevation and curve radius. In fact, it would be conceptually difficult to classify and take into consideration these sections; that is the reason why transition lengths have been introduced only in the calculation of the length of curves, by assigning half-length to the curve part and half-length to the straight part or to the other adjacent section in the case of consecutive curves. For all the missing transition lengths, the information of which were not available, a reasonable length has been introduced on the basis the maximum allowable roll speed $\Omega \leq 0.038 \, \text{rad s}^{-1}$ and the maximum allowable derivative of the non-compensated acceleration (Equation (13)), equal to $\Psi \leq 0.35 \, \text{m s}^{-3}$ (see below) for the rank to which the vehicle belongs. The instantaneous non-compensated acceleration for a railway vehicle
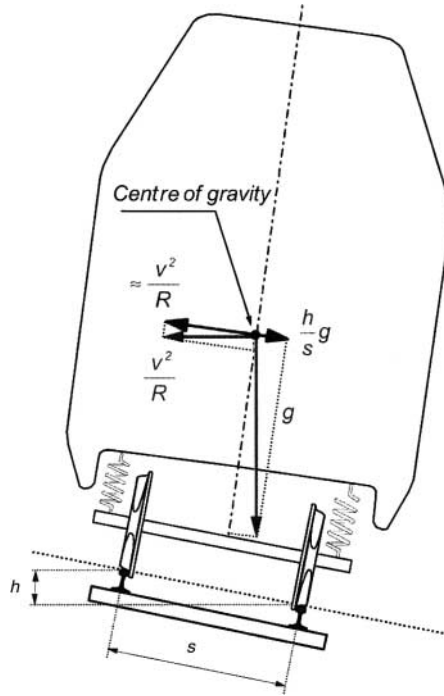
Figure 5. Accelerations in curve.

running in a curve (Figure 5) and the expressions of Ω and Ψ are defined as

$$a_{\mathrm{nc}} = \frac{V^2}{R} - g\frac{h}{s_t}, \quad \Omega \cong \frac{\Delta h \cdot V}{s_t l}, \quad \Psi \cong \frac{V \cdot \Delta a_{\mathrm{nc}}}{l}; \tag{13}$$

where h is the superelevation height in mm, s_t is the nominal distance (1500 mm) between the two contact points on the wheelset when it is centred on the track, V represents the constant vehicle speed in transition sections (in m/s), Δa_{nc} (m/s^2) is the variation in non-compensated acceleration and l (in m) the length of the transition section. The two above-mentioned criteria can be satisfied at the same time by choosing an opportune value for the superelevation gradients $\mathrm{d}h/\mathrm{d}s$ with respect to the curvilinear abscissa s of the track in the range 1–1.5‰, considering that $\mathrm{d}h/\mathrm{d}s \cdot l \cong \Delta h$.

The further division of each radius class in superelevation classes has been arranged as listed below, by grouping the class of superelevation in five groups and choosing a few height value in each of them:

- 0;
- 10–40: 10, 20, 30, 40;
- 50–80: 50, 60, 70, 80;
- 90–120: 90, 100, 110, 120;
- 130–160: 130, 140, 150, 160;

since in reality the superelevation heights are usually rounded to the nearest centimetre. For the purpose of the dynamic simulations, each superelevation class is represented by the value (h_r) to which corresponds the highest sum of products between section lengths and number of weekly shifts.

	Superelevation (mm)															
	0	**10-40**				**50-80**				**90-120**				**130-160**			
Mean radius (m)	0	10	20	30	40	50	60	70	80	90	100	110	120	130	140	150	160
217	45	45	50	50	50	55	55	55	60	60	60	65	65	65	65	70	70
238	45	50	50	55	55	55	60	60	60	65	65	65	65	70	70	70	75
263	50	50	55	55	60	60	60	65	65	65	70	70	70	70	70	75	75
294	55	55	55	60	60	65	65	65	70	70	70	70	70	75	75	80	80
333	55	60	60	65	65	65	70	70	70	70	70	70	75	80	80	85	85
385	60	65	65	70	70	70	70	70	70	70	75	75	80	85	85	90	95
455	65	70	70	70	70	70	70	70	70	75	80	85	90	90	95	100	100
556	70	70	70	70	70	70	70	75	80	85	90	95	95	100	105	110	115
714	70	70	70	70	70	70	80	85	90	95	100	105	110	115	120	125	130
1000	70	70	70	70	75	85	90	100	105	115	120	125	130	135	140	145	150
1667	70	70	70	85	95	110	120	130	140	145	155	160	160	160			
5000	70	85	120	145	160												

Figure 6. B-rank speed table: values of speed V_r as a function of radius curve R_m and superelevation h_r.

3.2. *Determination of speed in each class*

As regard the speed V_r to be assigned to each track in the mean line, the choice has been made according to the table in Figure 6, which summarises the speeds in km h^{-1} to be observed by B-rank vehicles. In fact, there are four different rank classes in Italy (P, C, B and A, in the descending order of quality) which generally have to observe different speed limits in the same track.

For each combination of curve radius and superelevation, the speed is chosen sufficiently high, according to a certain criterion: as depicted in the speed table, three criteria (corresponding to different sectors of the table) are taken into account. In order to explain the procedure, first of all from Equation (13) can be derived the expression of the balancing speed $\hat{V}$ for which the non-compensated acceleration vanishes, being the centrifugal force exactly balanced by the component of the gravitational force along the tangent plane to the track:

$$a_{nc} = 0 \Rightarrow \hat{V} = \frac{Rgh}{s_t}. \tag{14}$$

After changing the units to have the track distance s_t in mm, the speed in km h^{-1} and the superelevation in mm, Equation (14) becomes

$$h = 11.8 \frac{\hat{V}^2}{R}; \tag{15}$$

also, by introducing the maximum allowable speed in the track V_r and a coefficient c, such that $\hat{V} = cV_r$, taking into account Equations (13)–(15), the following system can be written as follows:

$$h = \frac{11.8}{R}(cV_r)^2$$
$$a_{nc} = \frac{V_r^2}{12.96}(1 - c^2), \tag{16}$$

in which h and R are known, while the unknowns are V_r, c and a_{nc}.

By expressing s_t and h in mm, the radius curve R in m, the speeds V_r (in km/h) are chosen as clarified below:

Dark sky blue sector:

the speeds in this sector are chosen by setting $c = 0.8$ in the system (16) regardless of the resulting value of a_{nc}, so that the theoretical expression $\tilde{V}_r$ of the speed V_r becomes

$$\tilde{V}_r = 1.06\sqrt{\frac{Rh}{7.55}} \quad (\text{km/h}), \tag{17}$$

where the radius curve is in m and the height of superelevation is in mm; the height of superelevation is hence proportional to the centrifugal acceleration. The factor 1.06 means that the speed can be further increased by 6% with respect to the value included in the radical, because the vehicle belongs to the B-rank class. The effective speed for each radius-superelevation combination is then chosen as

$$V_r = \min(\tilde{V}_r, 130) \quad (\text{km/h}); \tag{18}$$

Yellow sector:

$$\tilde{V}_r = 3.6\sqrt{R\left(\frac{gh}{s_t} + 0.8\right)} \quad (\text{km/h}); \tag{19}$$

in the yellow part the $\tilde{V}_r$ speed of each subtrack is chosen according to Equation (19) after setting a non-compensated acceleration equal to $0.8\,\mathrm{m\,s^{-2}}$ in the system (16), regardless of the consequent value of c. The effective value has to be chosen as

$$V_r = \min(\tilde{V}_r, 70) \quad (\text{km/h}). \tag{20}$$

Light sky blue sector:

$$V_r = 70\,\text{km/h}; \tag{21}$$

this sector represents a connection zone between the two zones above mentioned. The speed is set equal to $70\,\mathrm{km\,h^{-1}}$ everywhere.

Regardless of the sector, the final speeds are finally rounded down to the nearest multiple of $5\,\mathrm{km\,h^{-1}}$.

3.3. *The Minuetto virtual track*

The application of the criteria explained in the previous section has provided the mean line reported in Table 6, made up of 34 classes (the non-existent radius-superelevation are not listed for brevity). For each subtrack, the mean radius R_r, the speed V_r, the superelevation h as well as the statistical weight p_k have been specified. This latter ($0 \le p_k \le 1$) is a weighting factor for the wear evaluation to take into consideration the frequency of each subtrack with respect to the whole set of the mean line under investigation.

3.4. *The worn rail profiles*

With respect to what has been presented thus far in setting-up the virtual track, detailed information about the track geometry have not been introduced yet: in particular, nothing has

Table 6. The Minuetto virtual track.

R_m (m)	R_M (m)	R_r (m)	h_{range} (mm)	h_r (mm)	V_r (km h^{-1})	p_k %
250	278	263	90–120	90	65	1.90
			130–160	160	75	4.21
278	313	294	90–120	90	70	1.11
			130–160	160	80	1.62
313	357	333	90–120	90	70	0.44
			130–160	140	80	1.24
357	417	385	50–80	50	70	0.80
			90–120	120	80	1.33
			130–160	150	90	4.17
417	500	455	50–80	80	70	1.44
			90–120	100	80	4.72
			130–160	130	90	1.29
500	625	556	10–40	10	70	0.14
			50–80	80	80	1.52
			90–120	90	85	2.01
			130–160	150	110	1.46
625	833	714	10–40	10	70	0.09
			50–80	70	85	1.56
			90–120	90	95	1.77
			130–160	130	115	0.78
833	1250	1000	10–40	10	70	1.10
			50–80	50	85	2.41
			90–120	120	130	2.16
			130–160	140	130	0.93
1250	2500	1667	0	0	70	0.17
			10–40	30	85	1.91
			50–80	80	130	1.68
			90–120	90	130	0.99
			130–160	150	130	0.17
2500	10,000	5000	0	0	70	1.08
			10–40	20	120	1.21
			50–80	50	130	0.25
			90–120	100	130	0.004
		∞				52.3

been said about the rail profile to be used in simulation. The simple hypothesis of a constant rail profile (a UIC60 rail profile for example) for all the tracks could be useful to overcome any conceptual difficulty in building a significant model of a railway net, but at the same time it can greatly reduce the validity of the results. In fact, the shape of the rails affects the position of the contact points both on rails and on wheels, the contact forces and, as consequence, the amount of wear and its distribution.

In this work, the available data on the rail profiles provided by RFI have been exploited to select a series of rail profiles to be used as time-independent profiles in the multibody simulations. According to the working hypothesis based on the collected data that in small radius curves it is easier to find a deeply worn rail profile than in straight tracks or in large radius curves, a pair of representative rail profiles, in a statistical sense, has been chosen for each radius curve range.

In detail, the population of the possible curve radius has been divided in 11 classes, coincident with the radius classes of the mean line previously described; for each rail class a left and right rail profile have been assigned. The choice of these profiles has been made by analysing the data concerning rails in different regions of Italy (Tuscany, Latium, Veneto, Trentino-Alto Adige and Sicily) and by calculating the average rail wear at 45°. Among the external rails,
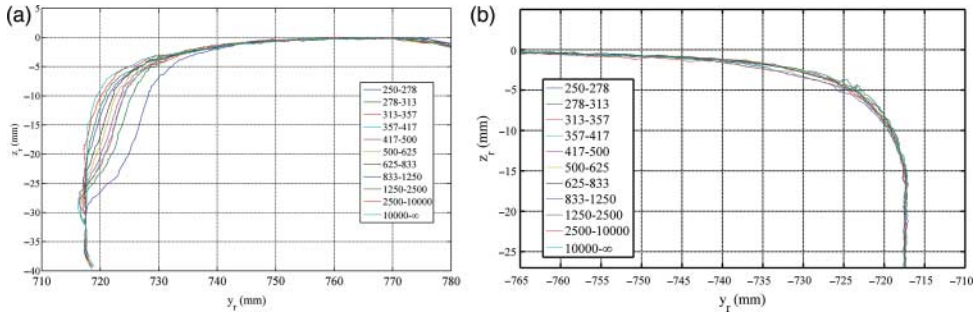
Figure 7. Worn rail profile of each class (cant of 1/20 rad). (a) External and (b) internal.

the profile with the minor deviation with respect to this average wear was selected as the representative external rail profile of the class, while the associated profile on the other side of the track was selected for the internal side of the track.

The rail profiles acquired by means of an optical instrumentation are shown in Figure 7(a) (the external rails) and 7(b) (the internal ones). The worn rail data included a certain amount of numerical noise and they had to be treated in order to smooth the profiles and their derivatives. To this end, the data were filtered with a sliding mean filter and then the rails profile have been rebuilt through several sections of cubic splines. Finally, these pairs of rail profiles have been associated with each class of the virtual track depending on the radius curve.

4. Description of the proposed wheel profiles

This section describes the procedures for the design of the two proposed wheel profiles, named CD1 and DR2 wheel profile. These procedures have been developed by the authors in collaboration with Trenitalia and RFI [5] in order to improve the poor performance with regard to the resistance to wear and the guidance in sharp curves that the S1002 wheel profile, originally designed to match the UIC60 rail profile canted at 1/40 rad) exhibits when coupled to the UIC60 rail profile canted at 1/20 rad.

4.1. *CD1 wheel profile*

The CD1 wheel profile has been designed through a discrete procedure in order to achieve two goals. The new wheel profile has to ensure an uniform distribution of the contact points in the flange zone in order to improve wear characteristics when matched to the UIC60 rail profile canted at 1/20 rad. In fact, wheel profiles with non-homogeneous contact points distribution involve a high wear rate and a high concentration of removed material, which is in turn characterised by an irregular distribution of the wear along the profile. Therefore, an uniform distribution of the contact points in the flange zone guarantees an improvement in wear behaviour of the wheel profile. Furthermore, CD1 wheel profile has been developed to get a target constant value of the equivalent conicity in a band around the nominal contact point (when the wheelset is in the neutral position).

The nomenclature and reference systems adopted for the wheel profile construction is shown in Figure 8. In the remainder of the present paper, the variables referred to the wheel and to the rail profile will be, respectively, signified by the subscripts w and r.

The design procedure developed to obtain the horizontal y_w and vertical z_w coordinates of the wheel profile starting from the coordinates y_r and z_r characterising the rail profile to match
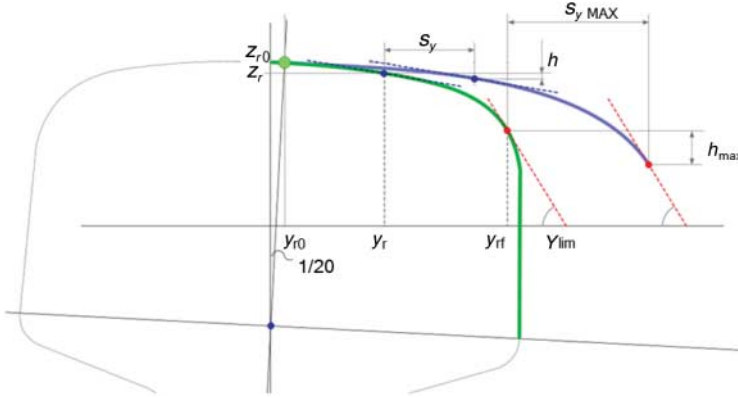
Figure 8.   Design procedure of the CD1 wheel profile.

is based on the following subsequent steps:

(1) computation of the coordinates y_w of the wheel profile;
(2) computation of the coordinates z_w of the wheel profile;
(3) completion of the resulting wheel profile with the extremity parts of ORE S1002 profile.

Step 1: Computation of the coordinates y_w

The range $[y_{r0}, y_{rf}]$, wherein the rail profile abscissa value y_r may vary, is discretised with a resolution equal to 0.1 mm. The relationship between the generic output abscissa value y_w characterising the points of the new wheel profile and the input y_r is chosen according to the following equation:

$$y_w = y_r(s_y) + s_y, \tag{22}$$

where the variable s_y represents the horizontal gap between wheel and rail profile and its value can vary from 0 to the maximum desired horizontal gap $s_{y\,MAX}$ and $y_r(s_y)$ is the relationship that occurs between s_y and y_r. This relationship, which can be chosen arbitrarily, has to satisfy the following boundary conditions:

$$y_{r0} = y_r(0) \quad y_{w0} = y_{r0},$$
$$y_{rf} = y_r(s_{y\,MAX}) \quad y_{wf} = y_{rf} + s_{y\,MAX}. \tag{23}$$

Considering the purposes previously described, the relationship adopted is the one shown in Figure 9. The horizontal part of this graphical illustration represents the purpose in maintaining a constant value of the conicity curve in a band around $y_r = 0$, while the increasing part determines the distribution of the contact points in the flange zone. Starting from the chosen $y_r(s_y)$, the abscissas y_w of the CD1 wheel profile are computed.

Step 2: Computation of the coordinates z_w

The vertical coordinate z_w value is evaluated from the corresponding rail value z_r, according to the following equation:

$$z_w = z_r(y_r(s_y)) - h(s_y), \tag{24}$$

where the $h(s_y)$ function is defined as

$$h(s_y) = -\int_0^{s_y} \tan\left(\gamma\left(y_r(s'_y)\right)\right) ds'_y. \tag{25}$$
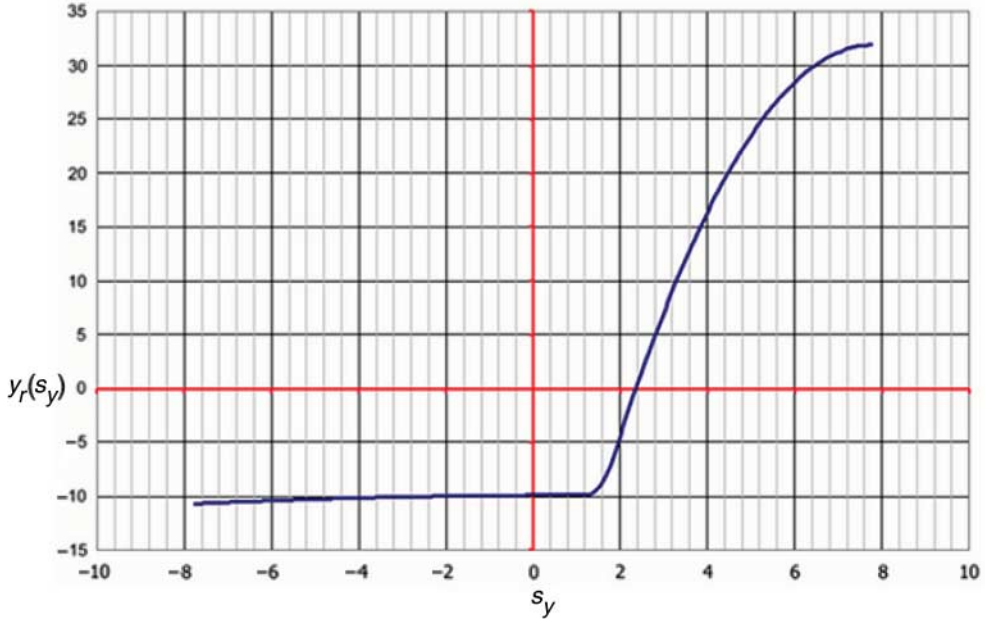
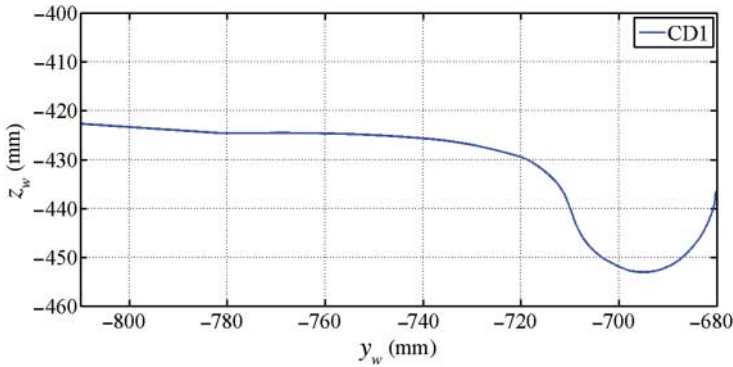Figure 9. Graphical representation of the function $y_r(s_y)$.

Figure 10. CD1 wheel profile.

The variable $\gamma(y_r(s'))$ represents the contact angle formed by the tangent to the rail profile in $y_r(s')$ and the horizontal plane. The following boundary conditions hold:

$$
\begin{aligned}
h(0) &= 0 \quad \gamma_0 = \gamma(y_{r0}) \quad z_{r0} = z_r(y_{r0}) \quad z_{w0} = z_{r0}, \\
h(s_{y\,\mathrm{MAX}}) &= h_{\max} \quad \gamma_{\lim} = \gamma(y_{rf}) \quad z_{rf} = z_f(y_{rf}) \quad z_{wf} = z_{rf} - h_{\mathrm{MAX}}.
\end{aligned}
\tag{26}
$$

Step 3: Completion of the resulting wheel profile

The CD1 extremities are designed connecting the resulting profile with the extremity parts of ORE S1002 profile through an interpolation process. Figure 10 illustrates the resulting CD1 wheel profile.
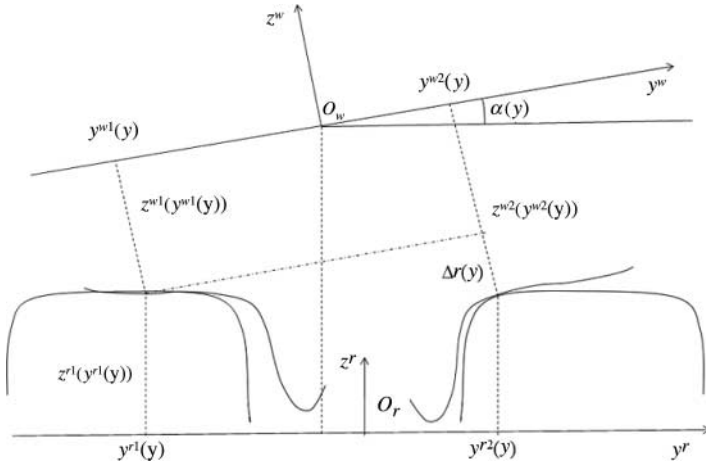
Figure 11. Adopted nomenclature for DR2 design.

4.2. *DR2 wheel profile*

The design of the DR2 wheel profile aims to guarantee the kinematic characteristics of the original matching formed by ORE S1002 wheel profile and UIC60 rail profile with laying angle α_p equal to $1/40$ rad, also with the new matching DR2 wheel profile – UIC60 rail profile canted at $1/20$ rad. The kinematic properties of the original matching have been chosen as reference value, because it is widely common in European railways and it is characterised by good performances in both wear and kinematic behaviour.

The procedure developed by the authors to design the DR2 wheel profile is articulated in several steps. A first intermediate wheel profile, conventionally named DR1, is designed according to the purposes previously described. The resulting rolling radii difference (RDD) function (the difference between rolling radii of the right and the left wheels for each lateral displacement y) is then compared with the one characterising the original wheel and rail profiles matching and a rolling radii difference error function is obtained. The minimisation of the error function through an appropriate algorithm leads then to the optimised version of the wheel profile, conventionally named DR2.

The design of the DR2 profile requires the introduction of two appropriate reference systems, namely the rail (or auxiliary) reference system $O_r x_r y_r z_r$ and the wheel (or local) reference system $O_w x_w y_w z_w$, both shown in Figure 11. The longitudinal axis x_r of the rail reference system is built tangent to the track centreline in the point O_r, while the z_r axis is normal to the rails plane. The origin O_w of the wheel reference system coincides with the centre of mass G_w of the wheelset. The x_w axis is parallel to the $x_r y_r$ plane and the y_w axis is coincident with the rotation axis of the wheelset.

The position of the local reference system origin expressed in the auxiliary reference system is denoted by

$$\mathbf{O}_w^r = [y \quad z(y)]^{\mathrm{T}}. \tag{27}$$

Introducing apexes 1 and 2 to denote, respectively, the right and left wheel, the coordinates of the contact points, respectively, in the auxiliary reference and the local reference system may be defined as

$$
\begin{aligned}
\mathbf{P}_c^{r1} &= [y^{r1}(y) \quad z^{r1}(y^{r1}(y))]^{\mathrm{T}} & \mathbf{P}_c^{w1} &= [y^{w1}(y) \quad z^{w1}(y^{w1}(y))]^{\mathrm{T}}, \\
\mathbf{P}_c^{r2} &= [y^{r2}(y) \quad z^{r2}(y^{r2}(y))]^{\mathrm{T}} & \mathbf{P}_c^{w2} &= [y^{w2}(y) \quad z^{w2}(y^{w2}(y))]^{\mathrm{T}}.
\end{aligned}
\tag{28}
$$

4.2.1. *Design of the DR1 wheel profile*

In the present research activity, the purpose in maintaining the kinematic properties of the ORE S1002-UIC60 canted at $1/40$ rad matching is achieved by imposing that some variables of the new matching (DR2 wheel profile – UIC60 matching canted at $1/20$ rad) remain the same of the original ones. More specifically, these variables (all depending on the wheelset lateral displacement y) are the lateral coordinates y_{r1}, y_{r2} of the contact points expressed in the auxiliary reference system, the rail functions $z_{40}^{r1}(\bullet)$, $z_{40}^{r2}(\bullet)$, the vertical coordinate $z(y)$ and the roll angle $\alpha(y)$ of the wheelset. In the remaining of the article, the variables characterising the original matching and those referring to the new matching will be, respectively, denoted by the subscripts 40 and 20.

Consequently, the six inputs required by the design procedure from the old matching are $y_{40}^{r1}(y)$, $y_{40}^{r2}(y)$, $\alpha_{40}(y)$, z_{40}^{r}, $z_{40}^{r1}(\bullet)$, $z_{40}^{r2}(\bullet)$, while the two further inputs required from the new matching are $z_{20}^{r1}(\bullet)$, $z_{20}^{r2}(\bullet)$.

The DR1 wheel profile design procedure is formed by the following steps:

(1) evaluation of the lateral $y_{20}^{w1}(y)$, $y_{20}^{w2}(y)$ and vertical $z_{20}^{w1}(y_{20}^{w1}(y))$, $z_{20}^{w2}(y_{20}^{w2}(y))$ coordinates of the contact points of the new wheel profile in the local reference system;
(2) filling of the hole regions of the resulting profiles;
(3) evaluation of the RDD functions characterising the new wheel profile.

Step 1: Evaluation of the lateral and vertical coordinates of the contact points of the new wheel profile

Starting from the inputs, the equations describing the coordinate transformation of the contact points between the local and the auxiliary reference system can be written both for the original matching:

$$\begin{pmatrix} y_{40}^{r1}(y) \\ z_{40}^{r1}(y_{40}^{r1}(y)) \end{pmatrix} = \begin{pmatrix} y \\ z_{40}(y) \end{pmatrix} + R(\alpha_{40}(y)) \begin{pmatrix} y_{40}^{w1}(y) \\ z_{40}^{w1}(y_{40}^{w1}(y)) \end{pmatrix}, \tag{29}$$

$$\begin{pmatrix} y_{40}^{r2}(y) \\ z_{40}^{r2}(y_{40}^{r2}(y)) \end{pmatrix} = \begin{pmatrix} y \\ z_{40}(y) \end{pmatrix} + R(\alpha_{40}(y)) \begin{pmatrix} y_{40}^{w2}(y) \\ z_{40}^{w2}(y_{40}^{w2}(y)) \end{pmatrix}, \tag{30}$$

and for the new matching:

$$\begin{pmatrix} y_{40}^{r1}(y) \\ z_{20}^{r1}(y_{40}^{r1}(y)) \end{pmatrix} = \begin{pmatrix} y \\ z_{40}(y) \end{pmatrix} + R(\alpha_{40}(y)) \begin{pmatrix} y_{20}^{w1}(y) \\ z_{20}^{w1}(y_{20}^{w1}(y)) \end{pmatrix}, \tag{31}$$

$$\begin{pmatrix} y_{40}^{r2}(y) \\ z_{20}^{r2}(y_{40}^{r2}(y)) \end{pmatrix} = \begin{pmatrix} y \\ z_{40}(y) \end{pmatrix} + R(\alpha_{40}(y)) \begin{pmatrix} y_{20}^{w2}(y) \\ z_{20}^{w2}(y_{20}^{w2}(y)) \end{pmatrix}, \tag{32}$$

where the wheelset lateral displacement value y is bounded in the range $[-y_M, y_M]$. The outputs of the design procedure that characterise the new wheel profile are the lateral $y_{20}^{w1}(y)$, $y_{20}^{w2}(y)$ and vertical $z_{20}^{w1}(y_{20}^{w1}(y))$, $z_{20}^{w2}(y_{20}^{w2}(y))$ coordinates of the contact points of the new wheel profile in the local reference system. The design procedure is performed in a discrete way for every y value of the discretised range $[-y_M, y_M]$ (with a resolution equal to 0.1 mm).

Step 2: Filling of the hole regions of the resulting profiles

The profile resulting from the previous step is characterised by holes (Figure 12(a)) that are regions where there is not any computed contact point. In the present procedure, these regions have been filled fitting the computed points with spline functions and the resulting wheel profile, named DR1, is illustrated in Figure 12(b).
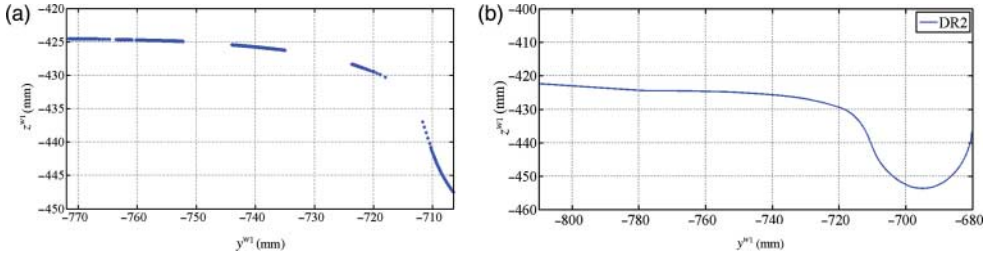
Figure 12. DR1 wheel profile design. (a) Contact points distribution and (b) DR1 wheel profile.
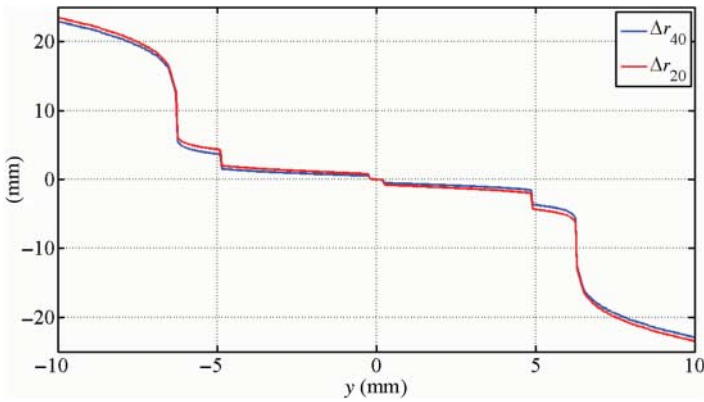

Figure 13. Rolling radii differences: $\Delta r_{20} = z_{20}^{w2}(y_{20}^{w2}(y)) - z_{20}^{w1}(y_{20}^{w1}(y))$ relative to the matching DR1-UIC60 canted at 1/20 rad and $\Delta r_{40} = z_{40}^{w2}(y_{40}^{w2}(y)) - z_{40}^{w1}(y_{40}^{w1}(y))$ relative to the ORE S1002-UIC 60 rail canted at 1/40 rad.

Step 3: Evaluation of the RDD functions characterising the new wheel profile

The RDD functions characterising the original (ORE S1002 wheel profile and UIC60 canted at 1/40 rad) and the resulting matching are, respectively, defined through the following expressions (Figure 13):

$$\Delta r_{40} = z_{40}^{w2}(y_{40}^{w2}(y)) - z_{40}^{w1}(y_{40}^{w1}(y)) \quad \Delta r_{20} = z_{20}^{w2}(y_{20}^{w2}(y)) - z_{20}^{w1}(y_{20}^{w1}(y)). \tag{33}$$

The adopted design procedure implies that the rolling radii difference of the output matching is equal to the one characterising the original matching, disregarding a small estimable variation $e = \Delta r_{20} - \Delta r_{40}$ (Figure 14), calculated by means of an appropriate analytical procedure.

4.2.2. *Optimisation of the wheel profile and design of DR2 wheel profile*

In order to improve the rolling radii difference error between the original matching and DR1 wheel profile – UIC60 canted at 1/20 rad matching, an optimisation algorithm has been developed according to the following steps:

(1) expression of the rolling radii functions variation between the new and the original matching as a function of the wheelset lateral displacement;
(2) minimisation process of the RDD function error to evaluate the optimum translation $k(y)$ and translation of the lateral input coordinates $y_{40}^{r1}(y)$, $y_{40}^{r2}(y)$ of the quantity $k(y)$;
(3) optimisation process and re-definition of the resulting lateral coordinates of the contact points in the auxiliary reference system;
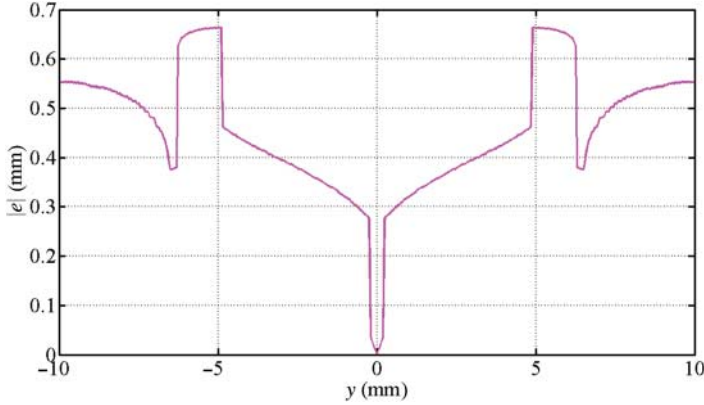(4) computation of the outputs characterising the optimised wheel profile;

Figure 14. Absolute value of the error e in rolling radii difference distribution for the DR1-UIC60 canted at 1/20 rad matching.

(5) holes fitting procedure;
(6) evaluation of the new RDD function.

Step 1: Expression of the rolling radii functions variation between the new and the original matching;

An expression of the RRD functions variation between the new and the original matching can be obtained. Subtracting Equation (29) from Equation (30) and Equation (31) from Equation (32), it leads to the following expressions:

$$\begin{pmatrix} y_{40}^{r2}(y) - y_{40}^{r1}(y) \\ z_{40}^{r2}(y_{40}^{r2}(y)) - z_{40}^{r1}(y_{40}^{r1}(y)) \end{pmatrix} = R(\alpha_{40}) \begin{pmatrix} y_{40}^{w2}(y) - y_{40}^{w1}(y) \\ \Delta r_{40} \end{pmatrix}, \tag{34}$$

$$\begin{pmatrix} y_{40}^{r2}(y) - y_{40}^{r1}(y) \\ z_{20}^{r2}(y_{40}^{r2}(y)) - z_{20}^{r1}(y_{40}^{r1}(y)) \end{pmatrix} = R(\alpha_{40}) \begin{pmatrix} y_{20}^{w2}(y) - y_{20}^{w1}(y) \\ \Delta r_{20} \end{pmatrix}. \tag{35}$$

Then, subtracting on turn Equation (34) from Equation (35) it holds

$$R^T(\alpha_{40}) \begin{pmatrix} 0 \\ \Delta z_{20}^r - \Delta z_{40}^r \end{pmatrix} = \begin{pmatrix} \Delta y_{20}^r - \Delta y_{40}^r \\ \Delta r_{20} - \Delta r_{40} \end{pmatrix}. \tag{36}$$

The second component of the previous equation leads to the expression of the rolling radii functions variation between the new and the original matching

$$(\Delta z_{20}^r - \Delta z_{40}^r)\cos\alpha_{40} = \Delta r_{20} - \Delta r_{40} = e(y) \tag{37}$$

as a function of the wheelset lateral displacement where $\Delta z_{20}^r = z_{20}^{r2}(y_{40}^{r2}(y)) - z_{20}^{r1}(y_{40}^{r1}(y))$ and Δz_{40}^r and $\Delta z_{40}^r = z_{40}^{r2}(y_{40}^{r2}(y)) - z_{40}^{r1}(y_{40}^{r1}(y))$.

Step 2: Minimisation process of the RDD function error to evaluate the quantity $k(y)$ and translation of the lateral input coordinates $y_{40}^{r1}(y)$, $y_{40}^{r2}(y)$ of the quantity $k(y)$;

The basic idea of this algorithm consists in translating the lateral input coordinates $y_{40}^{r1}(y)$, $y_{40}^{r2}(y)$ of a certain quantity $k(y)$, evaluated through a minimisation process of the RRD function error for each possible lateral wheelset displacement y. The lateral coordinates of the contact
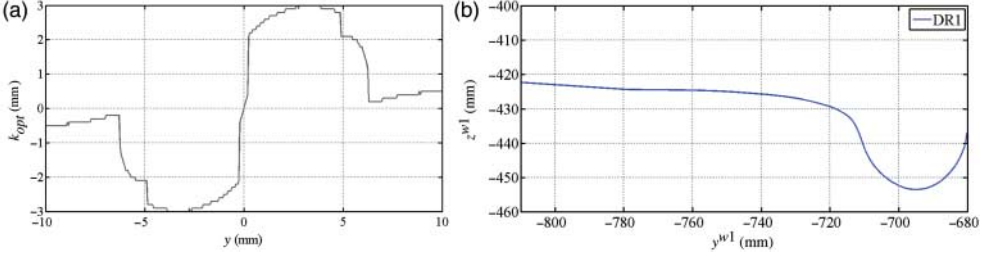
Figure 15. DR2 wheel profile design. (a) Optimal value of the translation quantity k and (b) DR2 wheel profile.

points in the auxiliary reference system can be then re-defined as

$$y_{40}^{r1\,k} = y_{40}^{r1} + k \quad y_{40}^{r2\,k} = y_{40}^{r2} + k, \tag{38}$$

where the k value is bounded in the range $[-\bar{k}, +\bar{k}] = I_k$. Therefore, the expression of the rolling radii error becomes a function of both y and k values:

$$E(y,k) = \cos \alpha_{40}(z_{20}^{r2}(y_{40}^{r2} + k) - z_{20}^{r1}(y_{40}^{r1} + k) - z_{40}^{r2}(y_{40}^{r2}) + z_{40}^{r1}(y_{40}^{r1})). \tag{39}$$

Equation (39) is used as the objective function to find the optimal value k_{opt} of the translation quantity, which is then defined for each wheelset lateral displacement y as

$$k_{\text{opt}}(y) = \arg \min_{k \in I_k} |E(y,k)|. \tag{40}$$

Step 3: Optimisation process and re-definition of the resulting lateral coordinates of the contact points in the auxiliary reference system;

The optimisation process is performed by discretising the I_k range with a resolution equal to 0.1 mm.

Figure 15(a) illustrates the graphical representation of the k_{opt} value for a determined lateral displacement y. It should be noticed that the resulting values are small compared to the characteristic length of the problem. The resulting lateral coordinates of the contact points in the auxiliary reference system are evaluated as

$$y_{\text{opt}}^{r1} = y_{40}^{r1} + k_{\text{opt}} \quad y_{\text{opt}}^{r2} = y_{40}^{r2} + k_{\text{opt}}. \tag{41}$$

Step 4: Computation of the outputs characterising the optimised wheel profile

Through the introduction of the resulting coordinates into Equations (32) and (31), the outputs $y_{20}^{w1}(y)$, $z_{20}^{w1}(y_{20}^{w1}(y))$, $y_{20}^{w2}(y)$, $z_{20}^{w2}(y_{20}^{w2}(y))$ of the optimised wheel profile-UIC60 rail canted at $1/40$ rad matching are given by the following expressions:

$$\begin{pmatrix} y_{\text{opt}}^{r1}(y) \\ z_{20}^{r1}(y_{\text{opt}}^{r1}(y)) \end{pmatrix} = \begin{pmatrix} y \\ z_{40}(y) \end{pmatrix} + R(\alpha_{40}(y)) \begin{pmatrix} y_{20}^{w1}(y) \\ z_{20}^{w1}(y_{20}^{w1}(y)) \end{pmatrix}, \tag{42}$$

$$\begin{pmatrix} y_{\text{opt}}^{r2}(y) \\ z_{20}^{r2}(y_{\text{opt}}^{r2}(y)) \end{pmatrix} = \begin{pmatrix} y \\ z_{40}(y) \end{pmatrix} + R(\alpha_{40}(y)) \begin{pmatrix} y_{20}^{w2}(y) \\ z_{20}^{w2}(y_{20}^{w2}(y)) \end{pmatrix}. \tag{43}$$

Step 5: Holes fitting procedure

The optimised wheel profile, obtained after the holes fitting procedure and named DR2 wheel profile, is shown in Figure 15(b).
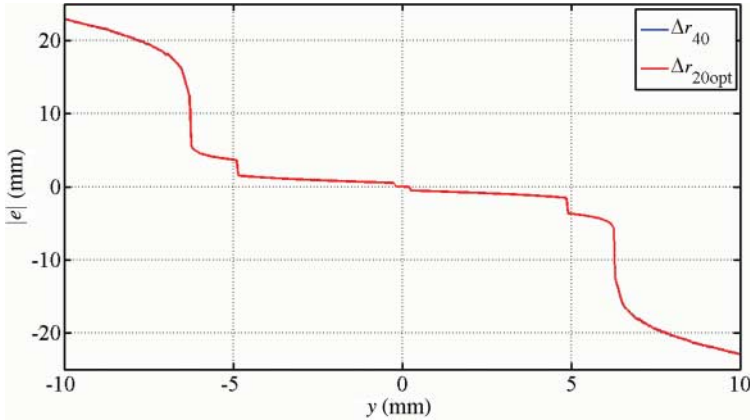
Figure 16. Rolling radii differences: $\Delta r_{20} = z_{20}^{w2}(y_{20}^{w2}(y)) - z_{20}^{w1}(y_{20}^{w1}(y))$ relative to the optimised matching DR2-UIC60 canted at 1/20 rad and $\Delta r_{40} = z_{40}^{w2}(y_{40}^{w2}(y)) - z_{40}^{w1}(y_{40}^{w1}(y))$ relative to the ORE S1002-UIC 60 rail canted at 1/40 rad.
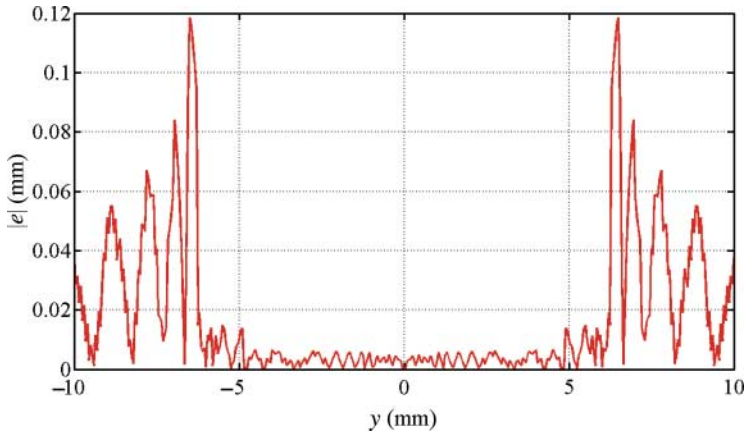

Figure 17. Absolute value of the error e in rolling radii difference distribution for the DR1-UIC60 canted at 1/20 rad matching.

Step 6: Evaluation of the new RDD function

The new RDD function is compared with the original one in Figure 16; it shows that the two plots are almost coincident and that the error (Figure 17), which depends on the discretisation precision of the range I_k, is about zero.

The design procedure adopted to define the DR2 discrete wheel profile may be affected by numerical errors coming from different sources such as

- use of splines in the holes (where there is not a contact point distribution) and of fictitious points at the extremities of the wheel profile (parts of the ORE S1002 have been used);
- subsequent re-interpolations and smooth process of profiles and derivatives of the wheel and the rail;
- since the DR2 wheel profile and UIC60 rail canted at 1/20 rad matching is based on the geometrical properties of the ORE S1002-UIC60 canted at 1/40 rad, it is characterised by the stiffness caused by the conformal contact typical of the original matching.

At the same time, one of the numerical advantage of the procedure consists in the fact that the new DR2 wheel profile is designed without any condition on the derivatives of the profiles;

this aspect involves a reduction of the smoothing requirements and does not further increase the ill-conditioning characteristic of the design problem.

4.3. *Comparison between the resulting wheel profiles*

As previously described, all the resulting profiles have been designed in order to obtain good kinematic and wear characteristics when matched with the UIC60 rail canted at $1/20$ rad. This section deals with the comparison of the CD1, DR1 and DR2 characteristics with those relative to the standard ORE S1002 (optimised to match the UIC60 rail canted at $1/40$ rad). Figure 18 shows the comparison between the resulting CD1, DR1 and DR2 wheel profiles and the original ORE S1002, while in Figure 19, their relative differences along the vertical coordinates are plotted.

The derivatives of the resulting CD1, DR1 and DR2 wheel profile compared with the derivative of the standard ORE S1002 are illustrated in Figure 20.

Differences in CD1 and DR2 wheel profiles properties coherently reproduce the fact that they have been produced with two different design aims and procedures. The DR1 and DR2 wheel profiles are instead almost coincident, representing that the DR2 optimisation algorithm may improve the DR1 designing procedure which nevertheless, produces itself a wheel profile with good kinematic and wear characteristics. It can be noticed that the new DR1 and DR2-UIC60 canted at $1/20$ matching try to reproduce the conformal contact characterising the original matching ORE S1002-UIC60 canted at $1/40$ with coherent vertical translations of
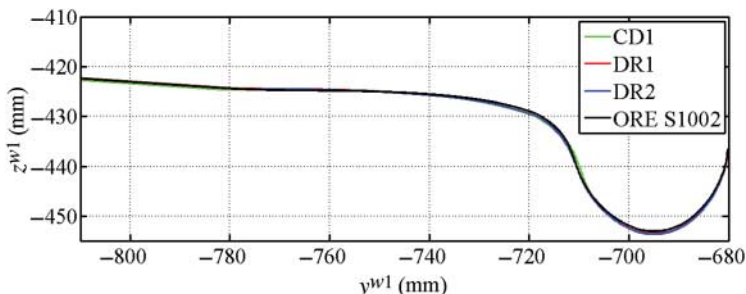
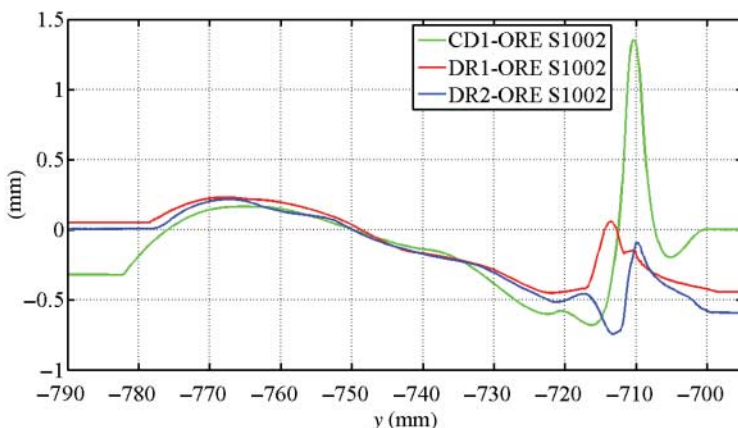Figure 18.   CD1, DR1, DR2 and ORE S1002 wheel profiles.

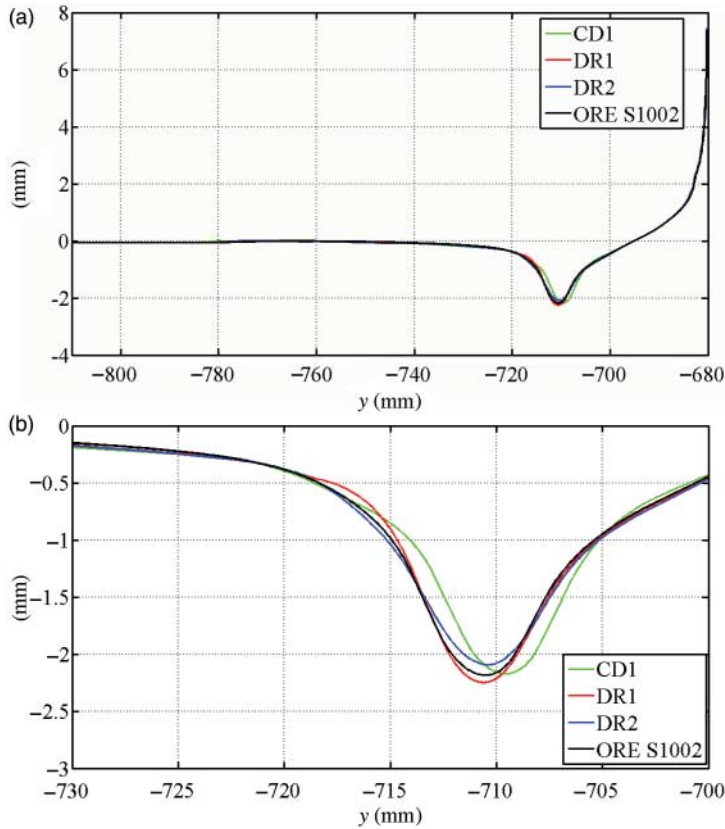Figure 19.   CD1, DR1, DR2 and ORE S1002 wheel profile derivatives.

Figure 20. Comparison of the four wheel profiles. (a) Tread zone and (b) flange zone.

the wheel profiles and derivatives in the tread and flange zone. More specifically, the points of the new wheel profiles in the tread zone (Figure 21(a)) are translated upwards with respect to those characterising the original ORE S1002 wheel profile, while the points in the flange zone slope downwards (Figure 21(b)).

5.   Wear control parameters

According to the current European Standard EN 15313,[8] the wear condition in a wheel can be evaluated through the measurement of three particular dimensions (the *qR* quota, the flange thickness *fT* and the flange height *fH*, Figure 22), without a complete detection of the two-dimensional profile. The three dimensions and the adopted nomenclature are defined as follows (Figure 22):

- the point P0 on the profile is 70 mm distant from the internal side of the wheel;
- the point P1 is 2 mm above the lowest point V of the flange on the wheel profile;
- the point P2 is 10 mm below P0 on the profile;
- the flange thickness *fT* is defined as the distance between P2 and the internal vertical side of the wheel; the *qR* is the horizontal distance between P1 and P0; the flange height *fH* is the vertical distance between P0 and V. P0 is also the point where the conventional rolling radius of a wheel is taken.

Because of the way the quotas are defined, they are positive and do not depend on the wheel rolling radius. The values of these parameters are measured periodically in order to decide whether the profile has to be re-turned or not (if it is still possible), considering the maximum or minimum values suggested by the current standard.[8] These limit values are reported in Figure 22.
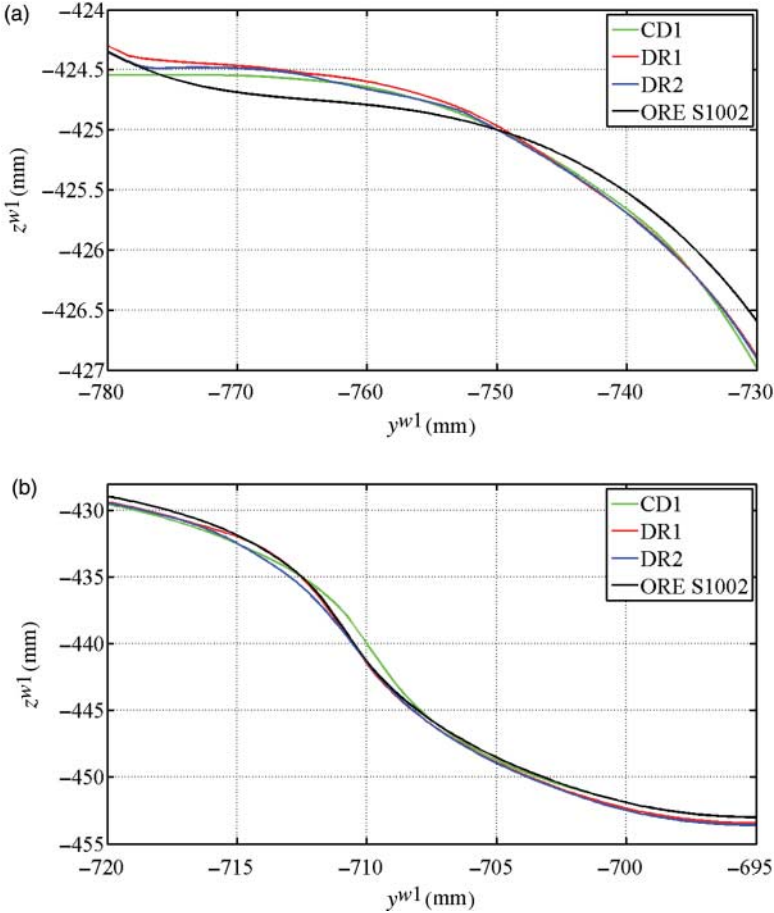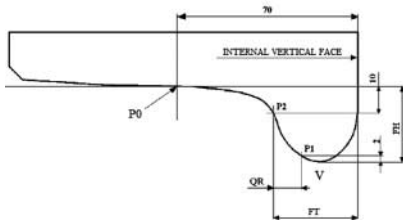

Figure 21.   Vertical differences CD1-ORE S1002, DR1-ORE S1002 and DR2-ORE S1002.

		$d \leq 630$	$630 < d \leq 760$	$760 < d$
fH	min	31.5	29.5	27.5
	max		36	

		$d \leq 760$	$760 < d \leq 840$	$840 < d$
fT	min	27.5	25	22
	max		33	

qR	min	6.5

Figure 22.   Reference dimensions of the wheel profile (left) and limit values in mm (right) for a wheel having an actual rolling diameter equal to d.

As regards their physical meaning, both the flange thickness *fT* and the flange height *fH* describe the size of the flange: variations of the first quota are due to the action of the wear which progressively reduces the thickness of the flange and its structural resistance, while the rise of the flange height is a measure of the wear on the tread. Conversely, the *qR* dimension is a shape parameter which quantifies the local conicity on the flange. The check of the wheel wear parameters enables the prediction of the consequences that wheel profiles wear determines on the dynamic behaviour of the railway vehicles. Even if running performances of a rail vehicle are ruled by the entire wheel–rail coupling and interaction, the control of wheel wear evolution (according to current Standards) represents an important aspect to avoid wear, stability or guidance problems.

6.   Wear analysis

In this section, the results of the dynamic simulations aimed at a wear evaluation will be presented in order to compare the profiles considered in this study: the standard S1002 and the two innovative profiles (CD1, DR2). For what concerns the resistance to wear, the performance can be assessed by analysing the evolution of three reference dimensions introduced in the previous section (5).

To this end, Figure 23 shows the progress of the mean *qR* dimension for each profile: as it can be seen, the progress of the CD1 and DR2 profiles is slower than that of the S1002; in particular, the best performance is given by the DR2 profile. In fact, assuming a comparison limit equal to 7 mm, which is slightly above than the acceptable threshold value of 6.5 mm prescribed by the standard,[8] the trend of the DR2 shows that the comparison limit is reached with an increase in the covered distance by at least 30%.

With regard to the progress of the flange thickness *fT* depicted in Figure 24(a), the minimum value equal to 22 mm [8] is reached after covering about 80,000 km when the S1002 profile is adopted on the Minuetto; differently, with the new profiles the total covered distance can be extend up to 100,000 km and above. Different from the *qR*, in the reduction of the flange thickness, the difference between the performance provided by the CD1 and DR2 profile is about 5% only.

With regard to the flange height *fH*, the comparison is depicted in Figure 24(b): this quota usually increases owing to the wear on the tread of the profile. The trend of this dimension for
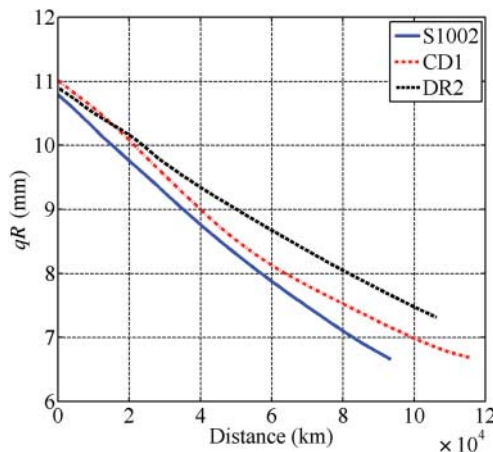

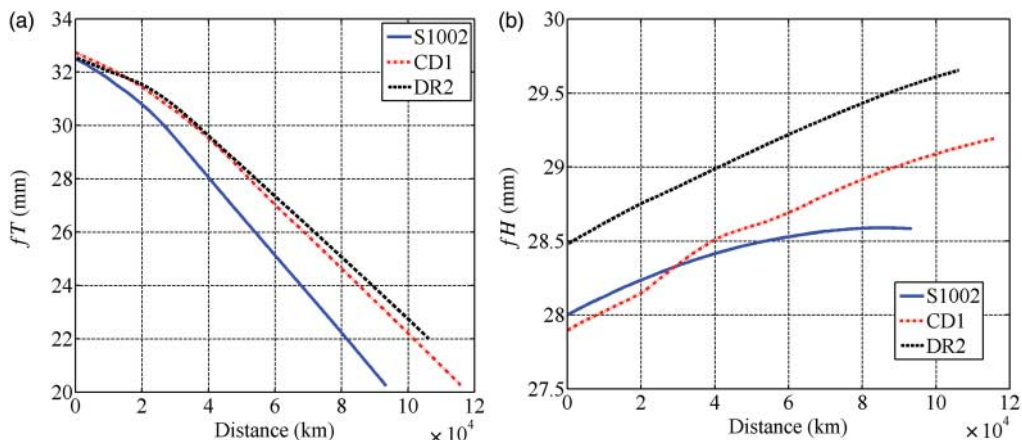Figure 23.   Progress of the *qR* dimension: comparison of the wheel profiles.

Figure 24.   Comparison of the wheel profiles. (a) Progress of the *fT* dimension and (b) progress of the *fH* dimension.
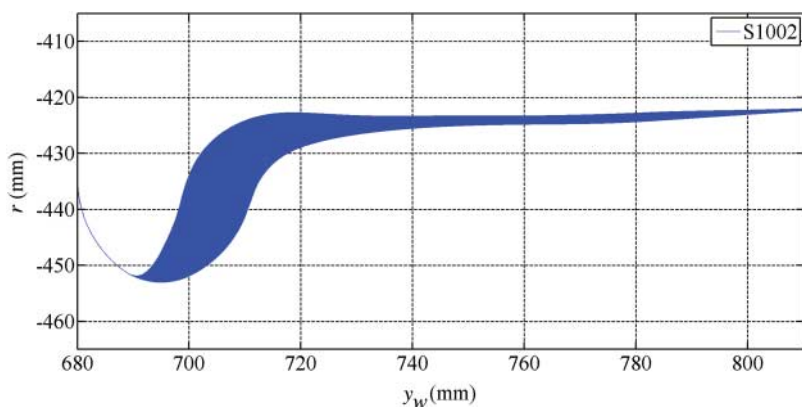

Figure 25.   Evolution of the S1002 wheel profile due to wear.

the two innovative wheel profiles is the same, except for an initial offset due to the different strategies with which they were generated. However, generally, the flange height progress is less important than the progress of the other dimensions (*fT* and *qR*) because it does not lead the wheel to a end-of-life condition.

With respect to the evolution of the wheel shape, the comparison between the initial and the final condition for the three profiles is presented in Figures 25–27. The variation in wheel profile is numerically described by means of about 100 procedure steps and besides the worn and the final profile, all the intermediate wheel geometries have also been plotted in the relative figure. Since the mean line of the Minuetto comprises a relevant percentage of sharp curves, the wear is mainly located on the flange instead of the tread.

7.   Stability assessment

Besides the resistance to wear, which is the main topic of the work, the performance of the new profiles has also been investigated from a running stability point of view in order to assess the critical speed of the vehicle, that is the minimum speed at which instability occurs by way of *hunting*. For a railway vehicle equipped with wheelsets instead of independent rotating wheels,
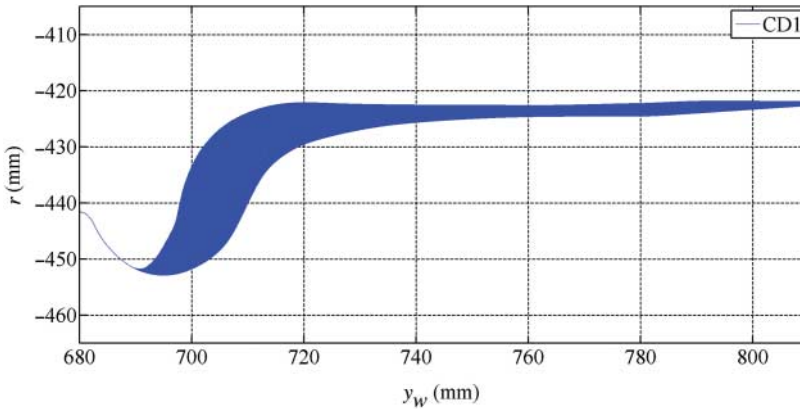
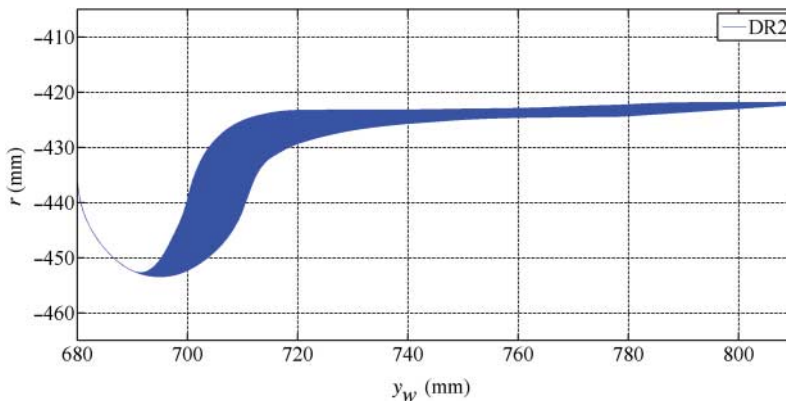Figure 26. Evolution of the CD1 wheel profile due to wear.

Figure 27. Evolution of the DR2 wheel profile due to wear.

a critical speed always exists and hence the maximum speed in service must be enough lower than this threshold.

It is also well-known that, besides the influence on wheel and rail wear, the characteristics of the wheel–rail interaction strongly affect both the guidance and the stability of a railway vehicle. More precisely, the influence of the wheel profile (or even better of the wheel–rail pair) lies in the rolling radius difference function: in fact, the progress of its first derivative is the local conicity of the wheel–rail pair and both the performance in negotiating the curves and the frequency of the wheelset kinematic oscillation depend on this conicity function. Leaving out the guidance which is not discussed in detail in this work, for what regards the stability at high speeds, the most simple evidence of this phenomenon can be found in Klingel's linear model of a wheelset on straight track.[26,27]

Nevertheless, being the physical problem nonlinear, not only for the characteristics of the wheel–rail coupling, but also for the structure of the vehicle, the better way to check the stability condition is a nonlinear approach by means of dynamic simulations. Among the most common methods used in investigating the critical speed via the numerical simulation of the vehicle motion,[28] a criterion based on the wheelset lateral displacement has been chosen in this work.

The procedure consists in simulating the initially perturbed motion of the vehicle on straight track at variable speed and checking the amplitude of the wheelset lateral displacement: the

vehicle can be considered stable at a certain speed if the lateral displacement of all its wheelsets is almost zero or anyway neglectable if compared with the flangeway clearance. In more detail, the result in this kind of test is a bifurcation diagram of the displacement amplitude as a function of the travelling speed; the two typical forms of the response are depicted in Figure 28, although more complicated situations may occur. Basically, in the supercritical case,
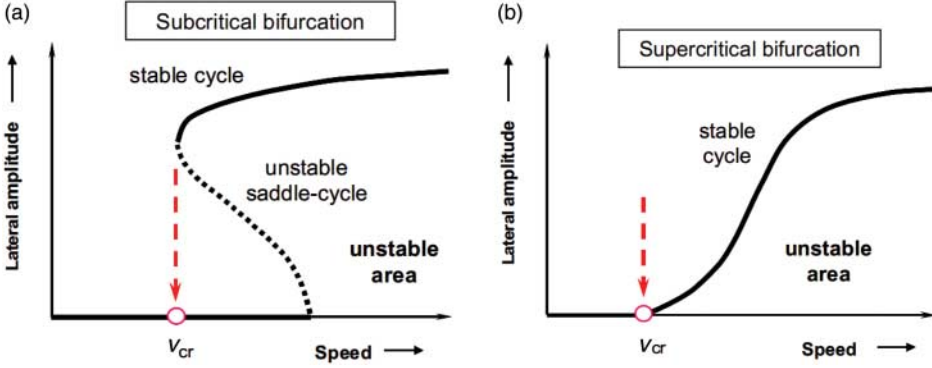

Figure 28.   Examples of bifurcation diagrams arising from stability tests.[27,29]
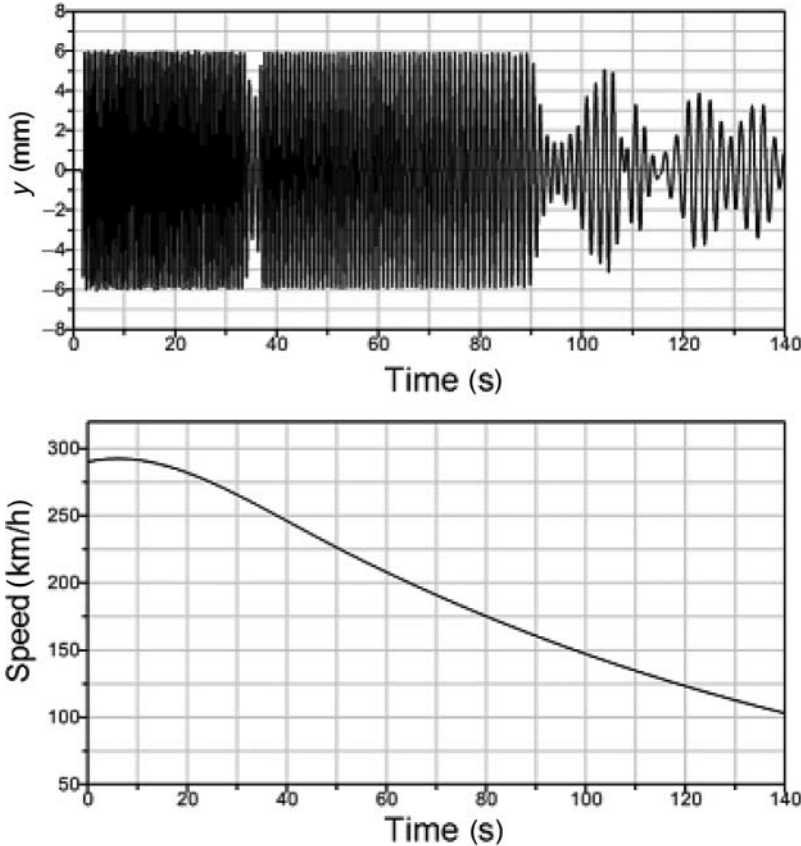

Figure 29.   Stability test of the unworn S1002 profile: lateral displacement of the seventh wheelset and speed profile.
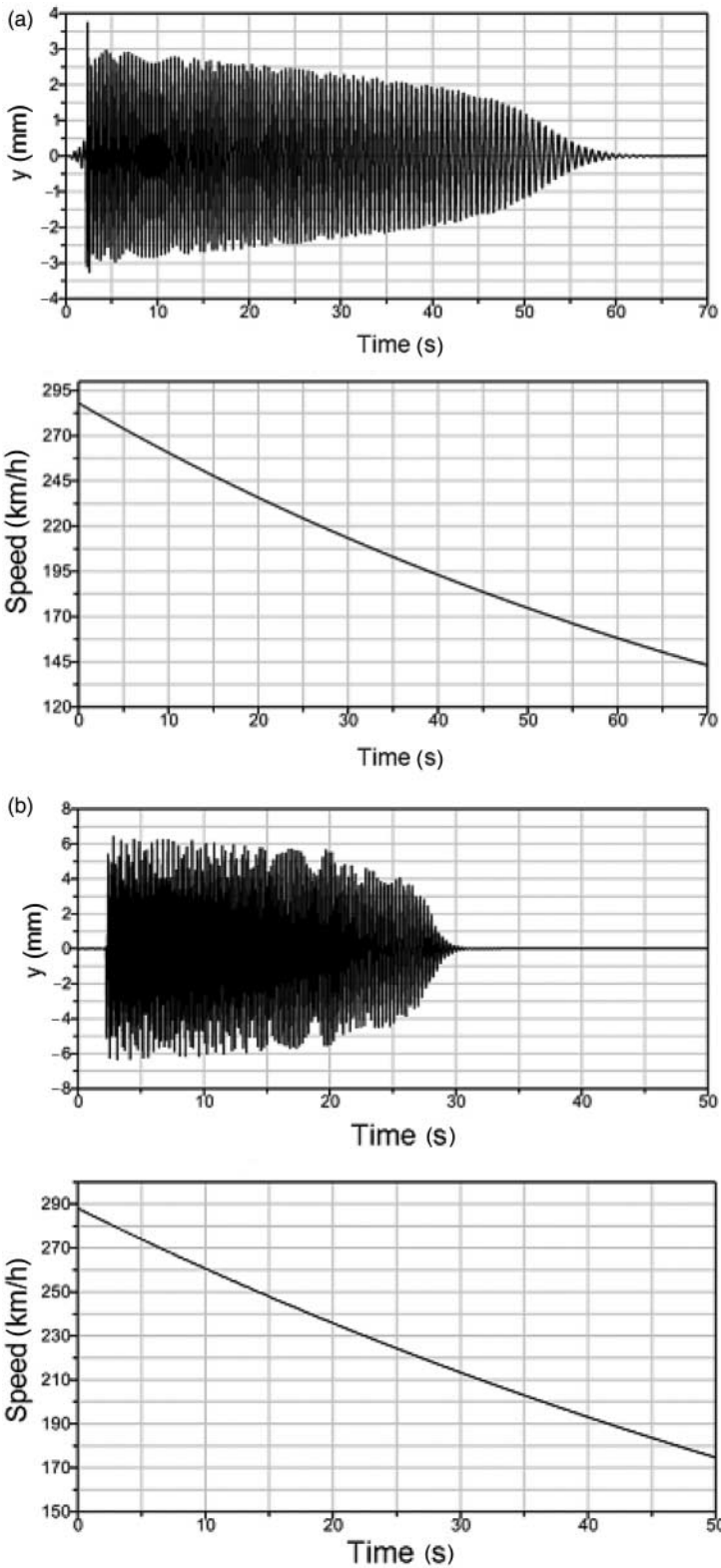
Figure 30. Stability test of the unworn profiles: lateral displacement and speed profile. (a) CD1 eighth wheelset and (b) DR2 seventh wheelset.

the amplitude increases continuously as the speed is augmented; on the contrary, when the bifurcation is subcritical, there is a speed range within which multiple solutions are possible depending on the amplitude of the excitation.

In order to find the real critical speed V_{cr}, the test should be carried out by reducing the travelling speed instead of increasing it, starting from an unstable running condition characterised by flange contact. The speed at which the lateral oscillation of the most critical wheelset vanishes or begin to reduce notably can be considered as the critical speed of the vehicle.

With regard to the present work, the stability assessment have been performed taking into account both the unworn and the worn geometries of the three wheel profiles. In particular, the wheel shapes corresponding to a covered distance equal to 80,000 km, being this latter the kilometrage at which the first limit value among the wear control parameters is reached (by the S1002 profile) and the reference mileage previously discussed for the wear comparison, have also been chosen as fully worn profiles.

The progresses of the lateral displacement of the most critical wheelset and the speed for each unworn wheel profile are reported in Figures 29, 30(a) and 30(b). In order to excite the lateral motion of the wheelsets and the flange contact, through a single-smoothed irregularity the track is suddenly displaced laterally of 5 mm before the reduction in speed takes place. In regarding to the friction coefficient at the wheel–rail contact, a value equal to 0.4 has been chosen to draw conservative conclusions.
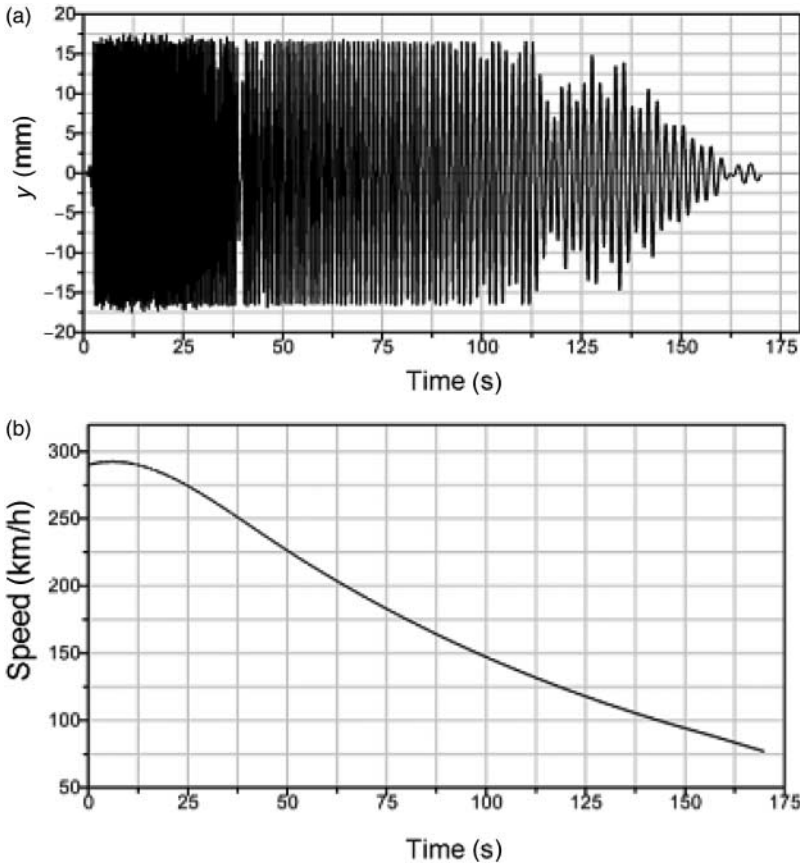

Figure 31.   Stability test of the worn S1002 profile: lateral displacement of the seventh wheelset.
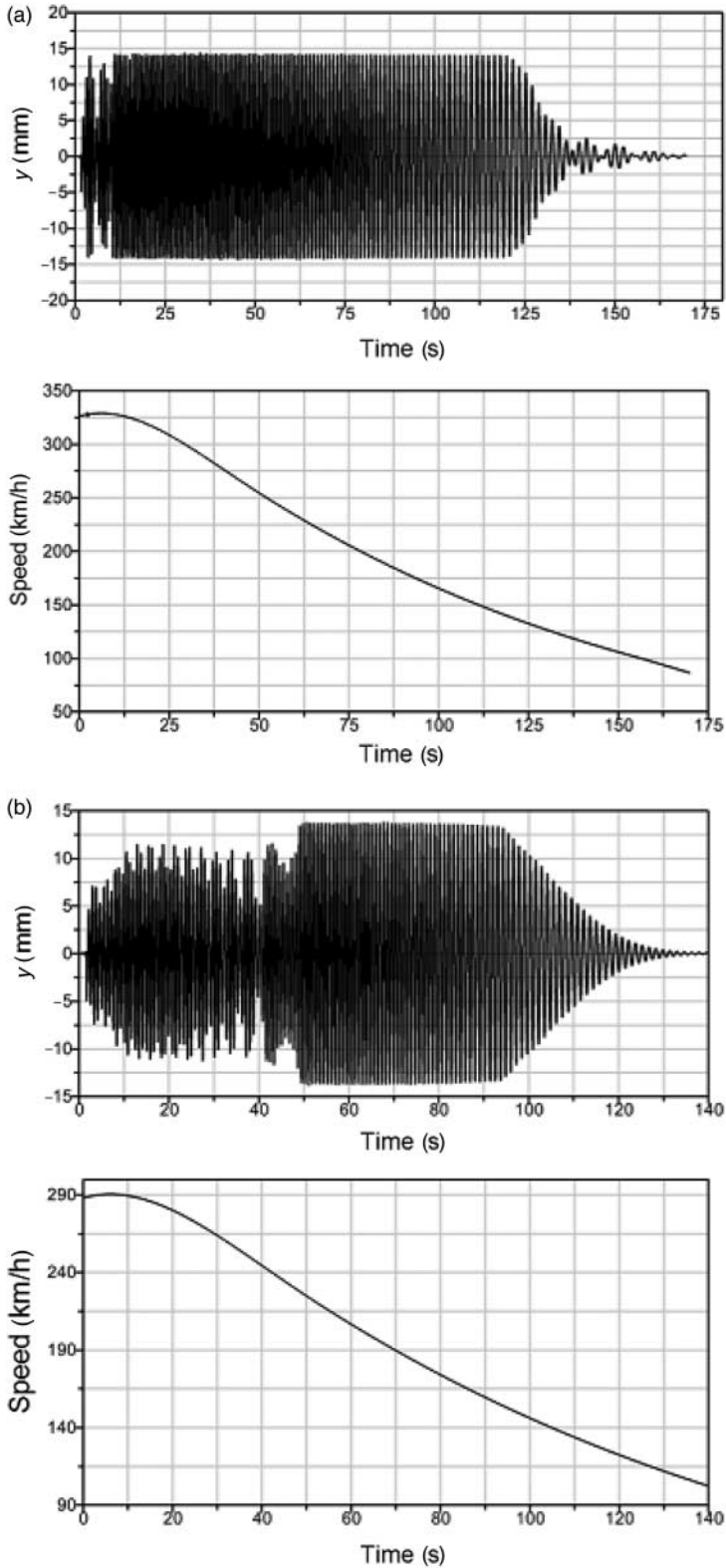
Figure 32. Stability test of the worn profiles: lateral displacement and speed profile. (a) CD1 eighth wheelset and (b) DR2 seventh wheelset.

Table 7. Summary of the critical speeds (km/h) of the Minuetto: comparison of the three wheel profiles after covering a few distances.

		Wheel profile		
		S1002	CD1	DR2
Covered distance (km)	0	155	>290	240
	29,000	125	170	160
	80,000	135	135	160

While the S1002 can be considered stable only for speed less than 155 km, both the new profiles have a critical speed greater than the maximum speed at the beginning of the simulation 290 km/h, which is considerably higher than the maximum service speed of the Minuetto, equal to 130 km.

The results of the stability test when the worn profiles are applied to the Minuetto are shown in Figures 31, 32(a) and 32(b). The critical speed are notably lower than the previous ones and the reduction in the oscillation amplitude convergence is slower.

Besides the unworn and worn geometries for each profile, the shapes corresponding to 29,000 km have also been tested. All the results of the stability assessment are summarised in Table 7: in all the investigated cases, the critical speeds arising from the employment of the two innovative profiles are greater than the maximum service speed of the vehicle.

8. Conclusions

In this paper, the authors presented a work focused on the development of a mathematical model for the wheel–rail wear evaluation in complex railway lines and on the comparison between the performance provided by different wheel profiles in terms of resistance to wear and running stability. More precisely, the standard ORE S1002 wheel profile, which is widely used on vehicles in service on the Italian railways, has been compared with two innovative wheel profiles developed by authors to improve the poor performance with regard to the resistance to wear and the guidance in sharp curves that the S1002 wheel profile exhibits when matched to the UIC60 rail profile canted at 1/20 rad).

The activity has been performed in collaboration with Trenitalia S.p.A and RFI which provided the necessary technical and experimental data for the implementation of the whole wear evaluation procedure.

The developed architecture is based on the mutual interaction between two main parts: a *vehicle model* responsible for the vehicle dynamics and a *wear model* for the evaluation of the amount and the distribution of material to be removed on wheels. The interaction between the vehicle dynamics and the wear model occurs at discrete steps and the evolution of the wheel geometry is reproduced through several intermediate profiles.

The entire procedure was validated in a previous work [6,7] by means of the experimental data, provided by RFI, regarding to the Aosta Pre-Saint Didier track and the ALn 501 'Minuetto vehicle'.

The developed model has been used in this work for a wear assessment on the ALn 501 Minuetto taking into account the whole Italian railway net in which these vehicles operate. The wear progress have been simulated on an equivalent statistical model of the complex railway, built by consulting the detailed database provided by RFI.

The two innovative wheel profiles developed in this activity for the UIC60 rail with a cant of 1/20 rad have proven to work fine as for the resistance to wear if compared with the S1002 wheel profile. In addition, the kinematic characteristics of these innovative wheel–rail

coupling are appreciably better than those of the S1002. A stability assessment have also been performed to check the critical speed of the Minuetto equipped with the wheel profile both in the unworn and worn condition.

Future developments of the present work will be based, first of all, on the experimental evaluation of the wear on the Minuetto equipped with the new wheel profiles by means of experimental tests that have been scheduled by Trenitalia, in order to verify the response in terms of progress of the reference dimensions.

To study the performance of the optimised wheel profile, also rail wear will be taken into account both from theoretical (wear model) and experimental (measurements performed by Trenitalia) standpoints.

Moreover, in the following phases of the present research activity, the wear model will be included in the optimisation loop of the wheel profile in such a way that the effects, from the wear standpoint, due to the geometric modifications of the profile can be directly evaluated.

Finally, as regards the wear model, further experimental laws could be introduced for a better simulation of the wear progress when other wear mechanisms are prevalent, such as the fatigue pitting wear and the plastic wear, both on the thread and flange zone.

Acknowledgements

References

[1] Polach O. Wheel profile design for target conicity and wide tread wear spreading. Wear. 2011;271:195–202.
[2] Esveld C, Markine V, Shevtsov IY. Shape optimization of a railway wheel profile. Eur Railw Rev. 2006;12(2): 81–86.
[3] Zakharov S, Goryacheva I, Bogdanov V, Pogorelov D, Zharov I, Yazykov V, Torskaya E, Soshenkov S. Problems with wheel and rail profiles selection and optimization. Wear. 2008;265:1266–1272.
[4] Persson I, Iwnicki S. Optimisation of railway wheel profiles using a genetic algorithm. Proc. 18th Int. Association for Vehicle System Dynamics Symp.; Kanagawa, Japan; 2003.
[5] Toni P. Ottimizzazione dei profili delle ruote su binario con posa 1/20. [Wheel profile optimization for UIC60 rails with laying angle equal to 1/20]. Florence: Trenitalia S.p.A.; 2010. Italian.
[6] Ignesti M, Malvezzi M, Marini L, Meli E, Rindi A. Development of a wear model for the prediction of wheel and rail profile evolution in railway systems. Wear. 2012;284–285:1–17.
[7] Auciello J, Ignesti M, Malvezzi M, Meli E, Rindi A. Development and validation of a wear model for the analysis of the wheel profile evolution in railway vehicles. Veh Syst Dyn. 2012;50(11):1707–1734.
[8] EN 15313. Railway applications – in-service wheelset operation requirements – in-service and off-vehicle wheelset maintenance. Bruxelles: European Committee for Standardization, 2010.
[9] Auciello J, Meli E, Falomi S, Malvezzi M. Dynamic simulation of railway vehicles: wheel/rail contact analysis. Veh Syst Dyn. 2009;47:867–899.
[10] Meli E, Falomi S, Malvezzi M, Rindi A. Determination of wheel–rail contact points with semianalytic methods. Multibody Syst Dyn. 2008;20:327–358.
[11] Kalker JJ. Three-dimensional elastic bodies in rolling contact. Dordrecht, Netherlands: Kluwer Academic Publishers; 1990.
[12] Kalker JJ. Survey of wheel–rail rolling contact theory. Veh Syst Dyn. 1979;8:317–358.
[13] Hertz H. The contact of elastic solids. J Reine Angew Math. 1881;92:156–171.
[14] Braghin F, Lewis R, Dwyer-Joyce RS, Bruni S. A mathematical model to predict railway wheel profile evolution due to wear. Wear. 2006;261:1253–1264.
[15] Enblom R, Berg M. Simulation of railway wheel profile development due to wear influence of disc braking and contact environment. Wear. 2005;258:1055–1063.
[16] Pombo J, Ambrosio J, Pereira M, Lewis R, Dwyer-Joyce R, Ariaudo C, Kuka N. A study on wear evaluation of railway wheels based on multibody dynamics and wear computation. Multibody Syst Dyn. 2010;24:347–366.
[17] Krause H, Poll G. Verschleißbei gleitender und wälzender Relativbewegung. [Analysis of the wear due to sliding and rolling relative motions]. Tribologie und Schmierungstechnik. 1984;31(4/5):209–214/285–289. German.

[18] Specht W. Beitrag zur rechnerischen Bestimmung des Rad- und Schienenverschleisses durch Gueterwagen. [A procedure for the analytical estimation of wheel and rail wear through freight wagon bogies]. Diss. Aachen: RWTH Aachen; 1985. German.

[19] Pombo J, Ambrosio J, Pereira M, Lewis R, Dwyer-Joyce R, Ariaudo C, Kuka N. Development of a wear prediction tool for steel railway wheels using three alternative wear functions. Wear. 2011;20:327–358.

[20] Pearce TG, Sherratt ND. Prediction of wheel profile wear. Wear. 1991;144:343–351.

[21] Zobory I. Prediction of wheel/rail profile wear. Veh Syst Dyn. 1997;28:221–259.

[22] Meli E, Magheri S, Malvezzi M. An innovative wheel–rail contact model for multibody applications. Wear. 2011;271:462–471.

[23] Magheri S, Malvezzi M, Meli E. Development and implementation of a differential elastic wheel–rail contact model for multibody applications. Veh Syst Dyn. 2011;49(6):969–1001.

[24] Kalker JJ. A fast algorithm for the simplified theory of rolling contact. Veh Syst Dyn. 1982;11:1–13.

[25] Oppenheim A. Schafer RW. Discrete-time signal processing. Englewoods, NJ: Prentice-Hall; 1989.

[26] Esveld C. Modern railway track. Delft, Netherlands: Delft University of Technology; 2001.

[27] Iwnicki S. The Manchester benchmarks for rail vehicle simulators. Lisse, Netherlands: Swets and Zeitlinger; 1999.

[28] EN 14363. Railway applications – testing for the acceptance of running characteristics of railway vehicles – testing of running behaviour and stationary tests. Bruxells: European Committee for standardization, 2010.

[29] Polach O. Influence of wheel/rail contact geometry on the behaviour of a railway vehicle at stability limit, August, The Netherlands; 2005;2203–2210.